Spatially-varying impedance model for locally reacting acoustic liners at a high sound intensity

Rémi Roncen, Fabien Méry, Estelle Piot, Patricia Klotz

Spatially-varying impedance model for locally reacting acoustic liners at a high sound intensity

Rémi Roncen [*1], Fabien Méry [†1], Estelle Piot [‡1], and Patricia Klotz [§2]

[1]ONERA /Département Multi-Physique pour l'Énergétique, Université de Toulouse, F-31055, Toulouse, France
[2]ONERA /Département Traitement de l'Information et Systèmes, Université de Toulouse, F-31055, Toulouse, France

Abstract

This paper is concerned with spatially-varying acoustic liner impedance in aeroacoustic ducts, in the presence of a high sound pressure level. It is shown that impedance discontinuity is a leading order parameter in the definition of the impedance variation. A large impedance discontinuity yields a high normal velocity variation, leading to significant nonlinear effects. An iterative numerical strategy is proposed to predict the spatially-varying acoustic impedance over a liner. A Bayesian inference process is coupled with a surrogate model to validate the model with measurements of the acoustic velocity fields above a liner at a high sound intensity, obtained using laser Doppler velocimetry.

Keywords: acoustic liner, high SPL, nonlinear impedance, spatially-varying impedance, impedance eduction, Bayesian inference

1 Introduction

Acoustic liners are passive devices typically used for noise control. They are usually mounted within the walls of complex systems subject to high sound intensities, such as an engine nacelle inlet or a car silencer, in an effort to absorb part of the noise. These acoustic liners are mostly locally reacting materials, made of a perforated face-sheet placed over a rigidly backed cavity. Due to the small scale of the perforations in acoustic liners, a detailed numerical investigation of the liner's efficiency would be too computationally expensive for industrial applications. A different approach consists in representing acoustic liners as a boundary condition, using the concept of impedance. Assuming that the liner can be treated macroscopically, the (surface) impedance is defined at each angular frequency ω as the ratio of the acoustic pressure p and the normal acoustic particle velocity v_n at a liner interface, as

$$Z(\omega) = \frac{p(\omega)}{Z_f v_n(\omega)} = r(\omega) + \mathrm{j}\chi(\omega), \tag{1}$$

with Z_f the characteristic impedance of air used as a normalization factor, $r(\omega)$ the resistance, $\chi(\omega)$ the reactance and j the complex unit. The impedance operator $Z(\omega)$, defined in the frequency domain as a function of the liner's geometric properties [1, 2], fully characterizes the acoustic behavior of the liner. The impedance is also a nonlinear function of the environment in which the liner is placed, i.e., it changes in the presence of a shear grazing flow and/or a high sound intensity. The accurate knowledge of the impedance across the entire frequency spectrum is crucial for the prediction of acoustic indicators related to complex systems.

By design, acoustic liners are predominantly used where a high sound pressure level (SPL) is expected. Due to the low percentage of open area in the liner facesheet, the acoustic velocity within the perforations can become high and local nonlinear effects can appear in the vicinity of the liner perforations even at a mild ambient SPL [3–8]. Detailed numerical simulations exploring this phenomenon have shown the transition from linear to nonlinear regimes [9–15], shedding more light on the absorption mechanisms of liners at a high SPL. It is now widely accepted that the phenomenon behind an SPL driven nonlinear behavior is related to the appearance of vortex-shedding mechanisms near the perforation aperture when the sound intensity is high enough, leading to a conversion from an (irrotational) acoustic energy into a (rotational) fluid kinetic energy.

[*]Corresponding author: remi.roncen@onera.fr
[†]fabien.mery@onera.fr
[‡]estelle.piot@onera.fr
[§]patricia.klotz@onera.fr

The measurement of the impedance of a liner subject to a shear grazing flow and a high sound pressure level remains a challenging topic [16]. These measurements are routinely performed in small scale aeroacoustic ducts. Having measured an acoustic field that has interacted with the liner, one can attempt to best fit a numerical solution (representing the duct) to the experimental data, by correctly changing the impedance value in the numerical code. The "true" liner impedance value is then assumed to be the one at the "best-fit scenario". This strategy, often coined *eduction*, belongs to the general category of finite dimension inverse problems [17]. Current eduction strategies typically rely on optimization algorithms to minimize the distance between numerical and experimental fields in an efficient manner (see e.g., [18, 19]). Direct approaches have also been developed to avoid the iterative and more costly nature of minimization procedures (see e.g., [20, 21]), albeit at the expense of more stringent hypotheses (i.e., a uniform flow hypothesis). Adopting a Bayesian framework for the quantification of uncertainties, an iterative strategy based on the Markov chain Monte Carlo (MCMC) approach has also been derived to evaluate the probability density function of the impedance [22, 23].

If properly designed, the liner absorbs some of the incident wave energy in a given frequency range, usually near the liner's resonance. As a result, the wave amplitude over the liner can drastically differ spatially. Since the liner has a nonlinear response with respect to sound intensity, the impedance becomes a spatially-varying function due to the local sound amplitude being distinct over the liner.

Eversman [24] developed an iterative harmonic finite element solver to update the impedance value locally, as a function of the pressure fields above the liner. It was shown that the pressure fields would converge in a few iterations, thus enabling the use of such a loop within an optimization solver for the design of a double-degree-of-freedom liner. Beck et al. [25] and Billard et al. [26] used a similar iterative strategy to match the impedance measurements obtained in a normal incidence tube configuration. Lafont et al. [27] showed that not accounting for the decrease in SPL above the liner during the eduction process could cause a bias in the educed resistance value. A straightforward heuristic was used in Ref. [27] to model the spatial variation of the impedance, i.e., a monotonously decreasing function of the real part of the resistance was taken, with a threshold value indicating the position above the liner at which no nonlinear effect would be triggered anymore. A decrease in the acoustic resistance can indeed be expected as the amplitude of the wave decreases on top of the liner, given the known nonlinear acoustic behavior of liners at normal incidence [6–8]. This strategy showed a potential reduction in the cost function that was used in the optimization algorithm, using laser Doppler velocimetry (LDV) particle velocity fields as observed data. This reduction was all the more significant in cases where a high SPL was concerned. Recently, Chen et al. [15, 28] performed direct numerical simulations for the in-duct propagation of waves over arrays of acoustic resonators, showing a spatial dependency of the impedance. Non-uniform impedance boundary conditions (BC), including both the resistance and the reactance, where showed to improve the sound propagation predictions.

This paper is mainly concerned with using Eversman's approach [24] in the context of an eduction process, where an iterative strategy is developed to predict the sound fields within a duct and the local nonlinear impedance field. Previous works on spatially-varying nonlinear impedance eduction used a geometric definition of the impedance spatial variation [27, 28], which restricts the use of the educed impedance in more complex systems. In addition, no uncertainty quantification was performed. This paper's objective is to remove these two limitations. The first goal is to develop a numerical strategy to evaluate the acoustic fields in the presence of a nonlinear impedance boundary condition (BC), while avoiding the need for an a priori geometrical definition of the spatial dependency of the impedance. The strategy is similar to that of Eversman's, except that only a single acoustic mode is considered for the convergence analysis. The main novelty of this work is that the normal acoustic velocity is directly considered to update the impedance BC and assess the convergence, instead of the pressure field. The second novelty of this work is an eduction strategy for the uncertainty quantification of the spatially-varying impedance, in keeping with what was done in Ref. [23] for the constant impedance case.

The direct problem for acoustic wave propagation is first derived in the harmonic regime in Sec. 2, to account for the nonlinear interaction between an acoustic liner and the surrounding acoustic field. In pursuing the analysis of the direct problem, additional findings were made relatively to the nature of nonlinear behaviors of liners at grazing incidence. A numerical investigation of the model is thus conducted in Sec. 3, where different model parameters are varied. In Sec. 4, an eduction strategy is coupled with uncertainty quantification theory to yield the credibility intervals of the spatially-varying impedance field. The eduction is realized on experiments performed in ONERA's B2A aeroacoustic bench. A presentation of the main conclusions is given in Sec. 5.

2 Evaluation of the spatially-varying impedance

The direct problem consists in numerically calculating the acoustic fields (pressure and velocity) in a grazing flow duct, in the presence of a liner. Only the plane wave mode is considered. A locally reacting liner is classically represented by an impedance BC, which can here vary as a function of space. The 2D linearized Euler equations (LEE) are solved

using a harmonic Discontinuous Galerkin (DG) scheme [19, 23], succinctly recalled in Sec. 2.1 for completeness. Any 3D effect is neglected. The strategy for evaluating the acoustic fields in the presence of a nonlinear impedance BC is detailed in Sec. 2.2.

A small scale aeroacoustic bench is considered (both for numerical and experimental investigations). A schematics of ONERA's B2A bench is shown in Fig. 1, along with the area where measurements can be performed (LDV). An example of the flow profile that is used in numerical simulations is also given, as well as the 2D numerical mesh (done in Gmsh [29]). The liner is located at the bottom wall ($y = 0$) and is 150 mm long. The duct cross-section is square with a size $H = 50$ mm.

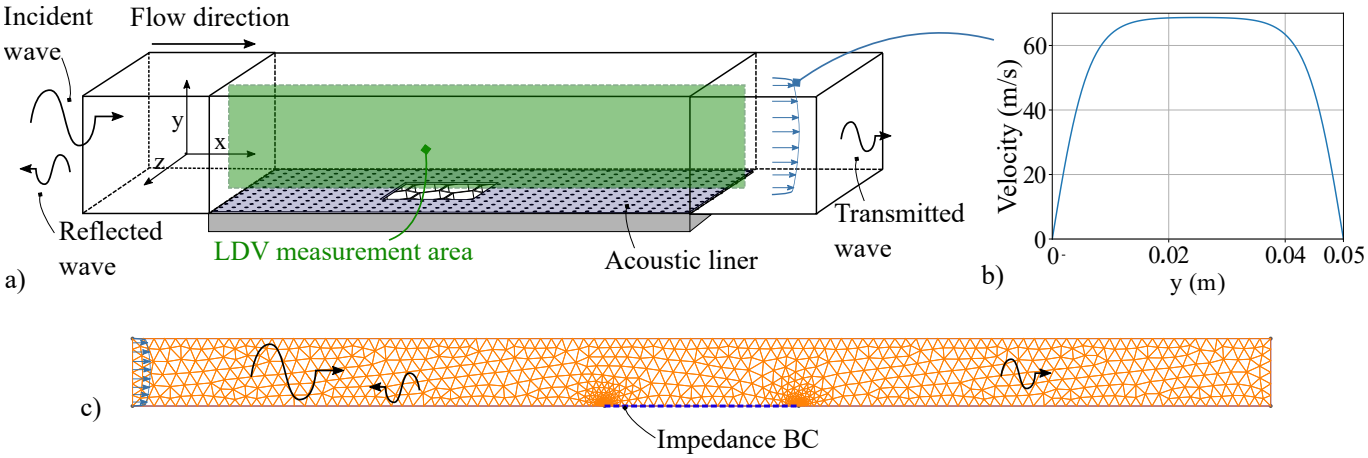

Figure 1: a) Schematics of the B2A aeroacoustic bench and LDV measurement area. b) Flow profile used in the simulations at Mach 0.2. c) Schematics of the mesh used throughout this study.

2.1 Linearized Euler equations with an impedance BC

The method description presented in this section is mostly inherited from our previous work in Ref. [23, II.B]. Only 2D simulations are considered in the present paper. They are carried out in the (x, y) plane at the center of the duct span (see Fig. 1).

The LEE, written in non-conservative form with an $e^{j\omega t}$ time dependence ($\omega = 2\pi f$, with f the frequency in Hz) are given by

$$\mathrm{j}\omega\boldsymbol{\varphi} + \boldsymbol{A}_x\partial_x\boldsymbol{\varphi} + \boldsymbol{A}_y\partial_y\boldsymbol{\varphi} + \boldsymbol{B}\boldsymbol{\varphi} = \boldsymbol{S}, \tag{2}$$

where, if a homentropic flow is assumed,

$$\boldsymbol{A}_x = \begin{pmatrix} U & 0 & c_0 \\ 0 & U & 0 \\ c_0 & 0 & U \end{pmatrix}, \ \boldsymbol{A}_y = \begin{pmatrix} V & 0 & 0 \\ 0 & V & c_0 \\ 0 & c_0 & V \end{pmatrix}, \ \boldsymbol{B} = \begin{pmatrix} \partial_x U & \partial_y U & 0 \\ \partial_x V & -\partial_x U & 0 \\ 0 & 0 & 0 \end{pmatrix}, \tag{3}$$

and with $\boldsymbol{S}$ a source vector. In this paper, plane acoustic waves of various incident SPLs are considered. In Eq. 3, U and V are the x and y components of the mean flow velocity, and c_0 the ambient fluid speed of sound. Components of the state vector $\boldsymbol{\varphi} = \left(u, v, \frac{p}{\rho_0 c_0}\right)$, where ρ_0 is the ambient fluid density, represent the acoustic perturbations around the mean flow, with u, v the x and y acoustic velocity, and p the acoustic pressure. Due to the homentropic flow hypothesis, the energy equation is replaced by the state equation $p = c_0^2\rho$, with ρ the density perturbation around ρ_0.

A shear mean flow profile with a null mean flow velocity at the walls is considered, so the impedance BC writes

$$p = \rho_0 c_0 Z v_n,$$

where v_n is the normal component of the acoustic velocity (pointing into the liner). The impedance Z is normalized by $\rho_0 c_0$ in this work. When a mean flow (U, V) is taken into account, $M_a = \frac{1}{Hc_0}\int_{y=0}^{y=H} U(y)\mathrm{d}y$ is the average (bulk) Mach number. The present study is restricted to incompressible mean flow.

A DG scheme is chosen to solve Eq. 2 and the associated BCs. Discontinuities are allowed at the interface between two elements, and the communication between elements is enforced via a numerical flux. An example of how such a method can handle discontinuities at hard-soft wall interfaces is found in Refs. [19, 30]. A flux vector splitting method is used to ensure the connection between interior cells, while a centered flux is chosen at the boundaries [19, 31]. To avoid aliasing errors that could cause instabilities when a shear grazing flow is present, high order quadrature rules are used (see e.g., Ref. [32, Sec. 5.3]).

2.2 Iterative calculation of the acoustic field

The strategy pertaining to the evaluation of acoustic fields and spatially-varying impedance is described in Sec. 2.2.1, and a first numerical application of the model is shown in Sec. 2.2.2.

2.2.1 General strategy

Assuming an incident SPL at a given frequency f, the following steps are taken to evaluate the spatially-varying impedance, and the acoustic fields:

1. A constant impedance is first considered, and an initial calculation is performed. This constant impedance is the reference one, when no SPL nonlinear effect is considered.
2. The normal acoustic velocity is evaluated on top of the liner (at the nodes of the BC mesh). This is in contrast with Eversman's strategy, where the pressure was used to evaluate a local particle velocity, using a plane wave hypothesis [24].
3. The spatially-varying nonlinear contribution to the impedance is evaluated, using the normal velocity at the BC as the input of a Melling- and Guess-like model [6, 7]; the impedance value is updated accordingly (see Eq. 5).
4. Another calculation is performed, with the updated spatially-varying impedance.
5. Steps 2 – 4 are repeated until convergence is reached.

To evaluate the convergence at step 5, an average distance d_i is defined and monitored between each successive iterations i and $i-1$ as

$$d_i = \frac{1}{N_{\mathrm{BC}}} \sum_{n=1}^{N_{\mathrm{BC}}} \left| Z_i\left(x_n\right) - Z_{i-1}\left(x_n\right) \right|, \tag{4}$$

where N_{BC} is the number of mesh nodes placed on the impedance BC, and x_n is the coordinate of the n^{th} node. A more detailed convergence study is postponed to Sec. 3.1.

In this model, no space-dependency is assumed a priori for the impedance field. Rather, the a priori is made on the model used to represent the relationship between a given liner and the acoustic velocity in its perforations. Here, it is assumed like in Refs. [6, 7] that the impedance can ultimately be written

$$Z_{\mathrm{NL}}\left(x\right) = Z_{\mathrm{ref}} + \alpha_{\mathrm{NL}} \left| v_n\left(x\right) \right|, \tag{5}$$

where Z_{ref} is the constant impedance value, when no SPL nonlinear effects are present (i.e., this is the initial value in step 1). Note that any nonlinear effect related to the presence of a shear grazing flow is integrated within Z_{ref}. The real parameter α_{NL} is a function of the facesheet porosity in Refs. [6, 7]. Here, α_{NL} is generalized by assuming a potentially unknown dependency on the material properties (we assumed $\alpha_{\mathrm{NL}} > 0$). Finally, $|v_n\left(x\right)|$ is the absolute value of the (spatially-varying) normal acoustic velocity at the impedance BC. Note that the approach followed here is general enough to allow the replacement of the nonlinear dependency in Eq. 5 by another model. A strong candidate model is Temiz's [8], due to its ability to also correct the imaginary part of the impedance (i.e., the reactance). Here the reactance will always be considered fixed for simplicity. Note that SPL nonlinear effects were shown to mostly happen near the resonance frequency [27, 33], where the reactance is null.

The proposed strategy aims at taking into account a nonlinear impedance BC in the harmonic regime. This amounts to approximating the impedance BC and its $|v_n\left(x\right)|$ dependency within a *linear* solver. The mathematical ground for such an approach is not immediately well-posed, and no claim is made here as to its validity, stability or even uniqueness of solution. However, the present nonlinearity is a "simple one", since the BC is reduced to a quadratic expression in $v_n(x)$. We are comforted in the reliability of the approach by our different numerical tests, convergence analyses, and by the results of Sec. 4 where the model is confronted to experiments. In addition, a similar study was conducted at normal incidence, showing excellent agreement with experimental data [25, 26].

2.2.2 Numerical example of the direct problem

Before carrying on with a detailed analysis of the model in Sec. 3, the investigation is first motivated by a succinct numerical example. A two-dimensional representation of the B2A aeroacoustic bench is considered numerically, with an incident wave of 140 dB at 1 kHz. The liner has a nonlinear factor of $\alpha_{\mathrm{NL}} = 1.2$ in Eq. 5, (for the Guess model [7], this is equivalent to taking a liner porosity of 5%). The absolute value of the normal component of the velocity field (v) above the liner is shown in Fig. 2, along with the corresponding impedance, in both cases with an initial

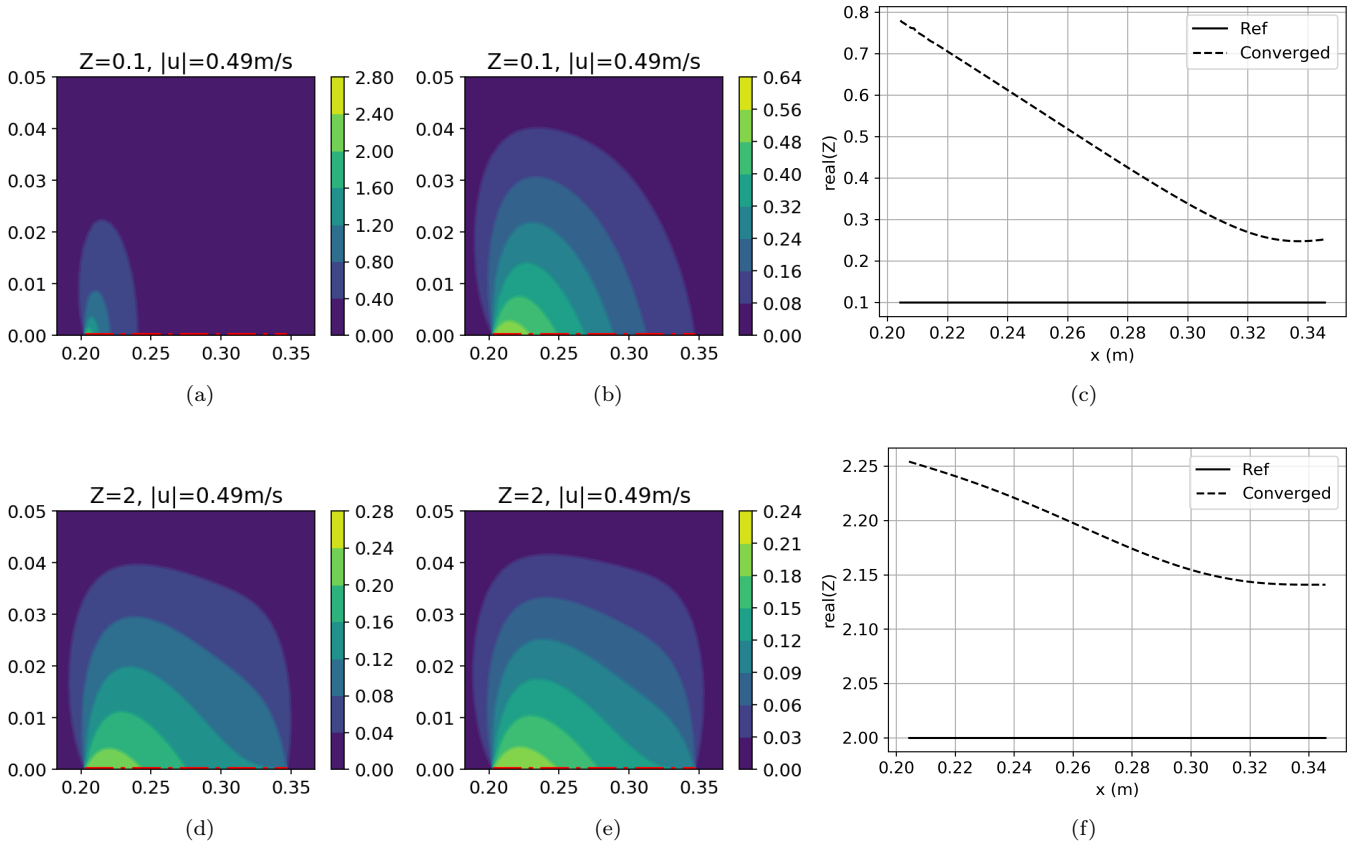

Figure 2: The $|v|$ field in the $x-y$ plane above a liner with constant and spatially-varying impedances (note the change in velocity scales between the figures). The dashed red line in the 2D plots corresponds to the position of the liner in the duct. No flow is considered. Incident SPL = 140 dB, $f = 1$ kHz, $\alpha_{\mathrm{NL}} = 1.2$. The incident wave is coming from the left (increasing x values). a) Initial $|v|$ field, $Z_{\mathrm{ref}} = 0.1$; b) Converged $|v|$ field, $Z_{\mathrm{ref}} = 0.1$; c) Initial and converged impedances, $Z_{\mathrm{ref}} = 0.1$; d) Initial $|v|$ field, $Z_{\mathrm{ref}} = 2$; e) Converged $|v|$ field, $Z_{\mathrm{ref}} = 2$; f) Initial and converged impedances, $Z_{\mathrm{ref}} = 2$.

constant impedance and a converged spatially-varying impedance. Two different reference impedances are chosen for the analysis, $Z_{\mathrm{ref}} = 0.1$ and $Z_{\mathrm{ref}} = 2$.

A few elements of interest observed in Fig. 2 are listed below:

- ▷ The converged spatially-varying impedance is a decreasing function of x, as expected [27].
- ▷ The initial velocity field can be very intense at the impedance discontinuity (left side of the liner). For the case with $Z_{\mathrm{ref}} = 0.1$, the v field becomes 5.7 times more intense than the incident velocity field (≈ 0.49 m/s at 140 dB) at the first discontinuity, if the impedance is assumed constant and equal to the linear value. This represents a local equivalent increase of about 15 dB.
- ▷ The phenomenon is not as marked at the downstream impedance discontinuity.
- ▷ The *converged* velocity field is less peaked near the upstream impedance discontinuity, since the $|v_n(x)|$ field is more smoothly spread over the liner.
- ▷ At a higher value of resistance ($Z_{\mathrm{ref}} = 2$), the peak intensity of the v field is lower, and the *converged* spatially-varying impedance is closer to the reference value.

The main finding of this first analysis is that an impedance discontinuity can drive a surge in the normal acoustic velocity field, thus leading to stronger nonlinear effects. This alters our previous general understanding, which was to ascribe the nonlinear contribution to the acoustic impedance as only a function of the local SPL on top of the liner, as done in Ref [24]. One should thus not use the SPL above the liner to evaluate the nonlinearity, but directly the normal velocity field (especially for low resistivity materials).

Taking two liners with the same nonlinear behavior at normal incidence (i.e., the same α_{NL}) results in a very distinct nonlinear behavior at grazing incidence, due to a different impedance discontinuity. The maximum increase in acoustic resistance is 0.7 when $Z_{\mathrm{ref}} = 0.1$, and only 0.25 when $Z_{\mathrm{ref}} = 2$.

3 Model investigation

This section investigates multiple aspects of the iterative model. The influence of the impedance discontinuity has already been partially shown in Sec. 2.2.2, and the influence of this discontinuity on the method *convergence* is further discussed in Sec. 3.1. The influence of a shear grazing flow on the converged impedance value is then evaluated, in both cases where the flow and acoustic source are in the same or opposite directions, in Sec. 3.2. Part of the analysis is performed again in Sec. 3.3 for an aeroacoustic bench having a lower or higher duct cross-section dimension, to assess whether the present results are sensitive to duct geometry. Finally, the outlet BC is considered partially reflective instead of fully anechoic in Sec. 3.4. This shows that the spatially-varying impedance is not necessarily a monotonously decreasing function of x, as previously expected [27, 28].

3.1 Influence of the impedance discontinuity on the convergence

Various "numerical" liners are considered. Despite having different reference acoustic resistances, the liners are assumed to follow the same nonlinear model and to have an identical $\alpha_{\mathrm{NL}} = 1.2$. The samples are considered at the resonance frequency, i.e., the imaginary part of the impedance is 0.

In Fig. 3, the convergence is carried out at 4 different reference impedances, with a maximum number of 50 iterations. Two different frequencies are considered during the analysis, 500 Hz and 1 kHz. Very similar results are observed in both cases.

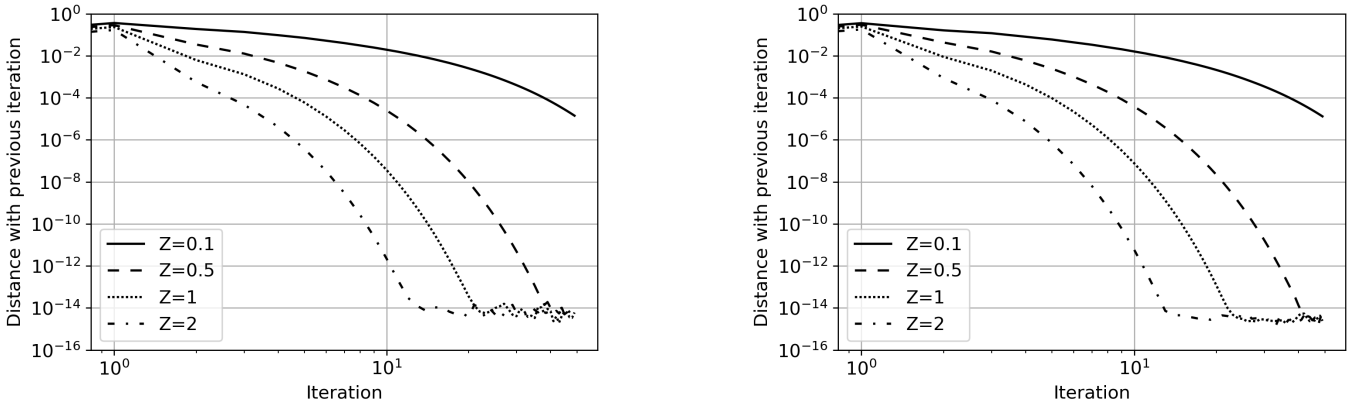

Figure 3: Convergence analysis of the spatially-varying impedance, for different reference impedances without flow, at different frequencies. Incident SPL = 140 dB. $\alpha_{\mathrm{NL}} = 1.2$. a) $f = 500$ Hz; b) $f = 1$ kHz.

For low reference values of the acoustic resistance, the convergence of the iterative process requires more iterations than for higher resistances. This is coherent with the observations made in Sec. 2.2.2. When the impedance discontinuity is large (i.e., for low resistances), the velocity field at the upstream discontinuity becomes more intense. This velocity field, in turns, feeds the nonlinear impedance model of Eq. 5. Due to the high value of the normal acoustic velocity, the acoustic resistance in the vicinity of the first impedance discontinuity is updated to a higher value. At the next iteration, the impedance discontinuity is thus less pronounced, which results in a smoother normal acoustic velocity field across the liner (as shown in Sec. 2.2.2), and less nonlinear effects than in the previous iteration. Due to the potentially strong variations of normal acoustic velocity fields at low resistances, over- and under-predictions of the impedance fields happen more when the reference impedance (resistance) is lower. This makes the convergence take longer, as seen in Fig. 4, where the first few iterations are shown for the spatially-varying impedance). It is thus not surprising that in Ref. [24], where high values of impedance were used (> 3), the convergence was reached within 5 iterations.

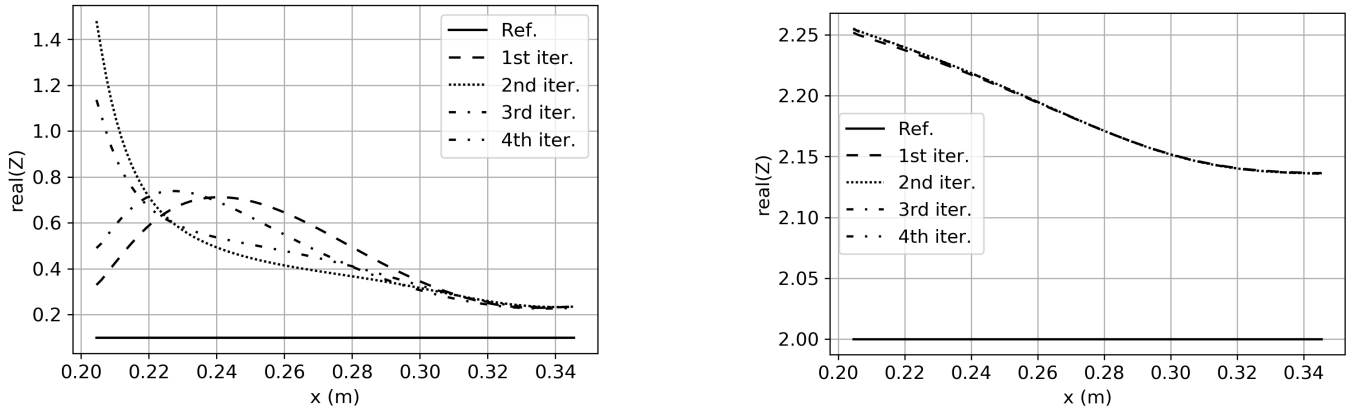

(a) (b)

Figure 4: Spatially-varying impedance at the first iterations. Incident SPL = 140 dB, $\alpha_{\mathrm{NL}} = 1.2$, $f = 1$ kHz. Converged impedance values were given in Fig. 2. a) $Z_{\mathrm{ref}} = 0.1$; b) $Z_{\mathrm{ref}} = 2$.

3.2 Influence of the Mach number

The influence of a shear grazing flow is considered here by varying the average Mach number M_a in the simulation, where the frequency is fixed at 1 kHz and the reference impedance at $Z_{\mathrm{ref}} = 0.5$, with an incident SPL of 140 dB. The direction of the flow can be changed artificially by setting a negative coefficient before M_a in the simulations. Three cases are considered, with $M_a = -0.2$, 0, 0.2. Only the converged absolute value of the y-direction particle velocity fields (v) is shown in Fig. 5. The flow profile shape is the one given in Fig. 1, where the analytical formulation of Rienstra was used [34], with a shear coefficient of 0.5. It is assumed that the liner impedance does not change with the Mach number value. The effect of the flow on the acoustic propagation in the lined duct is therefore restricted to convection and refraction effects. This assumption is made here in order to focus on the nonlinear effects created by the sound level onto the liner impedance.

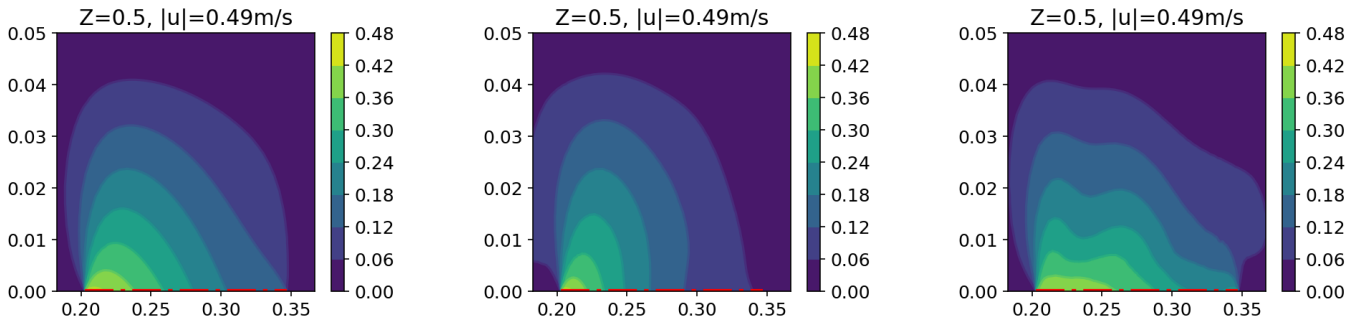

(a) (b) (c)

Figure 5: Converged $|v|$ fields in the $x - y$ plane at different Mach numbers. The reference impedance is $Z_{\mathrm{ref}} = 0.5$, and the frequency is $f = 1$ kHz, at an incident wave coming from the left with an incident SPL of 140 dB. This corresponds to an incident particle velocity of ≈ 0.49 m/s. The dashed red line represents the liner position in the duct. M_a is the average Mach number. a) $M_a = 0$; b) $M_a = -0.2$; c) $M_a = 0.2$.

Due to the various interactions between a wave and a shear grazing flow, the velocity fields of Fig. 5 are different. Specifically, when the wave and flow are opposite in direction, the $|v|$-field is more concentrated towards the upstream impedance discontinuity (i.e., the left side). However, the maximum value of the $|v|$-field does not seem to vary much between simulations (this was verified from $M_a = -0.5$ to $M_a = +0.5$ with 0.05 increments, and remains true for $Z_{\mathrm{ref}} = 0.1$, 0.5, 1, 2).

The converged impedances are shown in Fig. 6 for different Mach numbers and reference impedances.

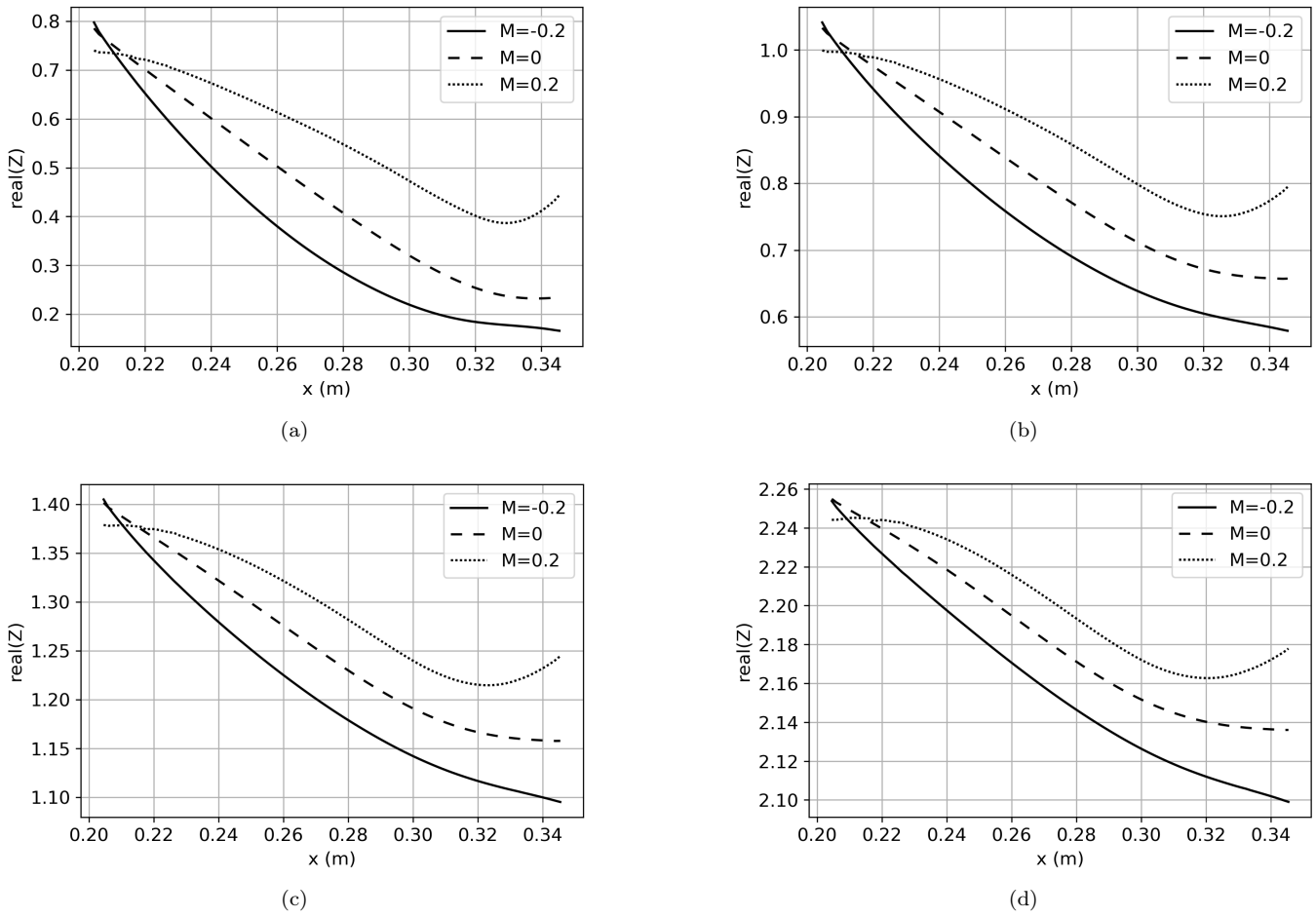

Figure 6: Converged spatially-varying impedances at different Mach numbers and different reference (constant) impedances. The incident wave comes from the left, with incident SPL = 140 dB, $f = 1$ kHz. For all cases, the nonlinear factor is $\alpha_{\mathrm{NL}} = 1.2$ in Eq. 5. a) $Z_{\mathrm{ref}} = 0.1$; b) $Z_{\mathrm{ref}} = 0.5$; c) $Z_{\mathrm{ref}} = 1$; d) $Z_{\mathrm{ref}} = 2$.

Whether the flow and the wave direction propagation are the same or opposite, similar values of the maximum impedance are obtained in Fig. 6. However, the nonlinearity has a less steep spatial decrease when flow and wave propagation share the same direction.

Potential reasons for this asymmetry are convective and refractive effects in presence of a shear flow. A wave going against the flow has a lower equivalent wavelength, due to convective effects. This can in turn increase the absorption (the wave effectively sees a longer liner), thus accelerating the rate of decrease of the nonlinearity. In addition, the same wave is refracted towards the direction of a positive gradient of the flow velocity (i.e., towards the centerline of the duct). This could be the reason why a lesser portion of the wave interacts nonlinearly with the impedance BC. The effects are reversed when the wave propagates in the same direction as the flow, thus leading to a relative increase in the nonlinear behavior. Since convective and refractive effects play an opposite role in the characterization of the liner efficiency, there might be some cases where the present conclusions do not hold anymore.

This analysis could be relevant to the current studies on the momentum-transfer/stress impedance [35, 36]. Indeed, it has been shown experimentally that the impedance eduction process yields a different result in the presence of a shear grazing flow, when the source direction is changed [37]. A minima, future eductions should now systematically report the incident SPL at which the measurements were performed, due to a potentially unforeseen bias caused by the impedance eduction process if no care is given to the space-dependency of the impedance. This bias, as highlighted by the present analysis, is caused by an asymmetry in $|v_n(x)|$ when considering different source directions relative to the flow. However, this divergence would mostly be present near the resonance, where such nonlinear effects are predominant.

Judging from Fig. 6, one could expect that an eduction process that only considers a constant impedance would yield an average value that is higher, for the resistance, in the case where the flow and incident wave are in the same direction. This difference would be exacerbated for low resistance materials.

In the presence of a high speed grazing flow, the liner's resistance is expected to increase [7, 38, 39], thus potentially reducing the space-dependency effect observed here. Note, however, that at low flow speeds, a reduction of the resistance value has sometimes been observed [40], which could in turn increase the sound-induced nonlinear effects at the impedance discontinuity.

3.3 Influence of bench geometry

All the numerical experiments previously shown have been carried out in a geometry representing ONERA's B2A aeroacoustic bench (Fig. 1). The main reason behind this choice is that an inverse problem is conducted with data acquired in this bench in Sec. 4. The influence of the bench geometry is now evaluated. A partial answer can be achieved by changing the duct height in our simulations, from 5 cm to 2 cm. Despite the increased spatial complexity of the mean flow and the potential issues associated with it, there may be an experimental benefit in having a duct of lower height, in that the cut-off frequency is higher (i.e., frequency above which higher order modes become propagative). Additionally, pressure measurements performed on the wall opposite the liner would now be closer to the liner, potentially facilitating the eduction strategy (but one could argue that placing microphones on the side of the bench would yield a similar result).

Converged impedances are shown in Fig. 7, where no flow is considered, with an incident wave of SPL 140 dB coming from the left, at a frequency of 1 kHz.

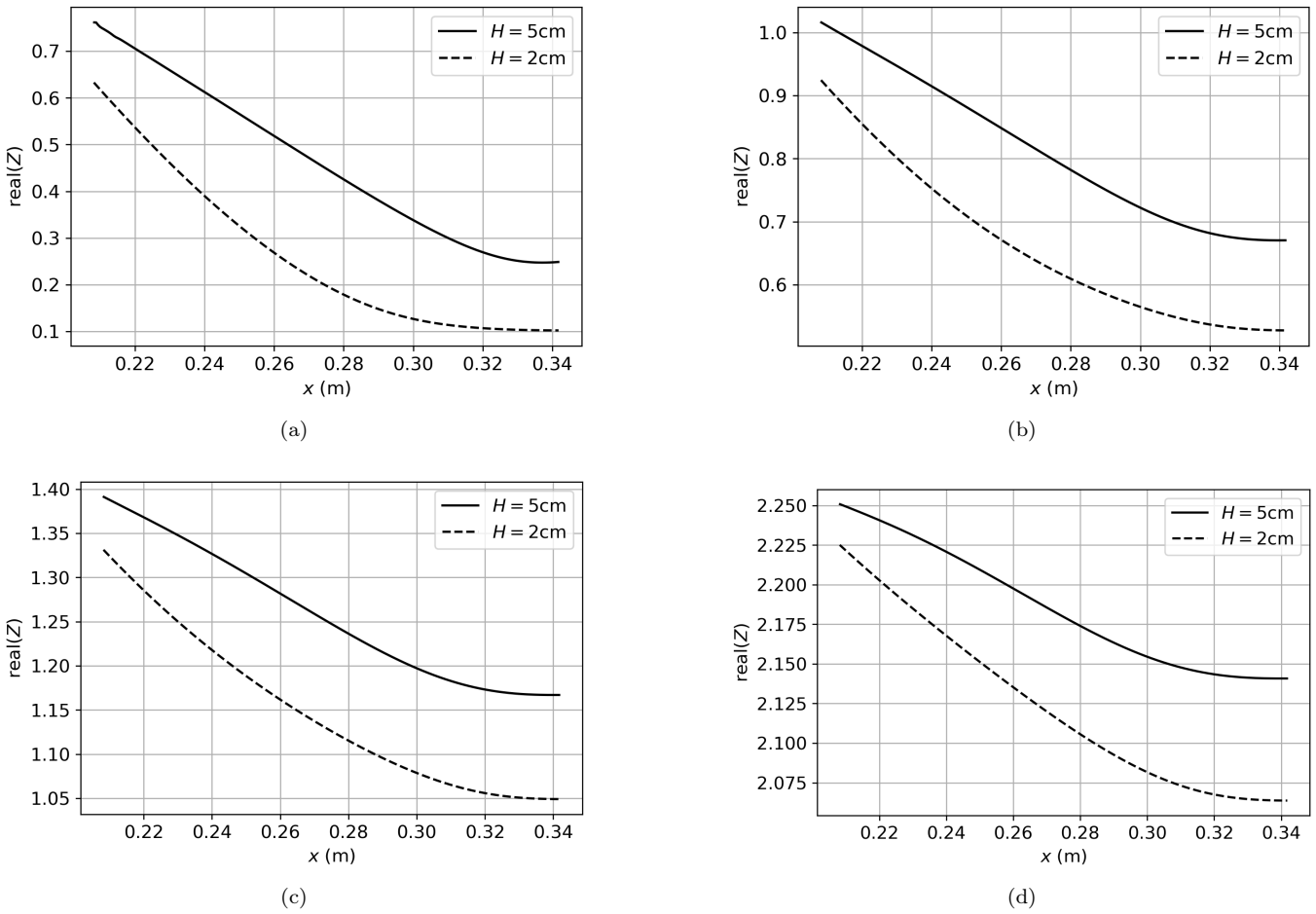

Figure 7: Converged spatially-varying impedances, without flow, for different duct heights H. Incident SPL = 140 dB, $f = 1$ kHz, $\alpha_{\mathrm{NL}} = 1.2$. a) $Z_{\mathrm{ref}} = 0.1$; b) $Z_{\mathrm{ref}} = 0.5$; c) $Z_{\mathrm{ref}} = 1$; d) $Z_{\mathrm{ref}} = 2$.

There are two main differences between the converged impedances, that appear independently of Z_{ref}. The spatial decrease is faster in the case where $H = 2$ cm, which can be explained by a stronger attenuation of the liner, within a more confined duct. The second difference is that the impedance value at the first discontinuity is lower in the case where $H = 2$ cm. A potential explanation for this effect is that due to the closer proximity with the upper wall, and

thus a boundary condition imposing $v_n = 0$, the $|v|$ field is more constrained than in the case where $H = 5\,\text{cm}$. In the limit where $H \to 0$ there appears a conflict, in that v needs to be high near the impedance discontinuity, and needs to be null at the upper wall. An average solution seems to be reached in practice.

To evaluate the above claim with more details, a numerical investigation is performed, in which the duct height H is varied more finely (down to 2 mm, up to 50 cm). The lower value of $H = 2\,\text{mm}$ is typically not encountered in practice and is only used here to get a sense of the limit of the observed phenomenon. For every simulation, convergence of the spatially-varying impedance is reached and the maximum value of the converged impedance is recorded (i.e., the value at the upstream impedance discontinuity). Results of the investigation are displayed in Fig. 8, for all 4 reference impedances, at incident SPL = 140 dB, $f = 1\,\text{kHz}$ and $\alpha_{\text{NL}} = 1.2$. The difference ΔZ between the maximum of the converged impedance and the reference one is shown.

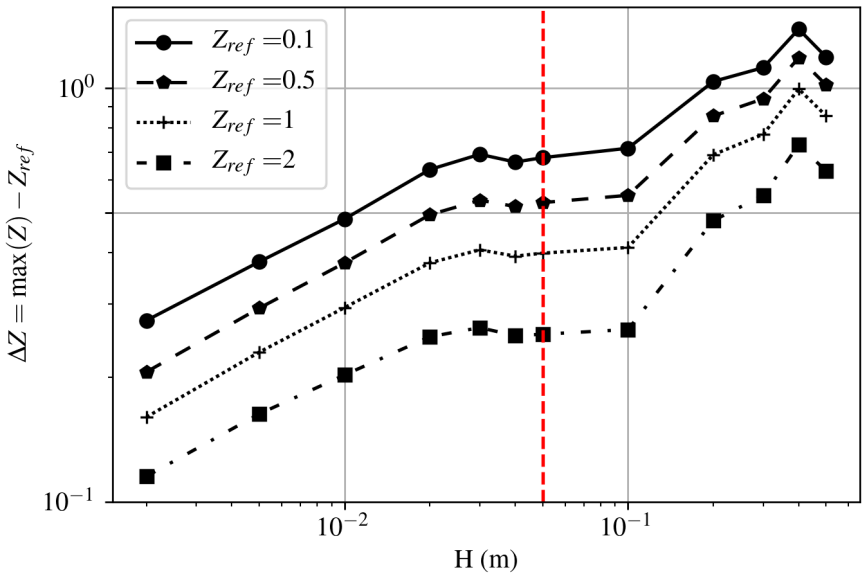

Figure 8: Difference between maximum of the spatially varying impedance and the reference one, as a function of the duct height H. Incident SPL = 140 dB, $f = 1\,\text{kHz}$, $\alpha_{\text{NL}} = 1.2$. The vertical red dashed line corresponds to $H = 5\,\text{cm}$, the duct height used in the remainder of this paper.

As expected from Sec. 2.2.2, ΔZ is greater for lower reference impedances. However, in agreement with the previous hypothesis, ΔZ is less pronounced when the duct height is smaller. More studies on this effect are warranted to evaluate the influence of a flow, since the flow profile is a complex function of the duct height. In particular, applications concerned with larger ducts (such as engine nacelles) should benefit from a more detailed analysis, since they seem to be more prone to a nonlinear behavior than smaller ducts.

3.4 Influence of a non-anechoic outlet BC

The general strategy allowing the calculation of the spatially-varying impedance does not enforce a monotonously decreasing resistance in the direction of the incident wave propagation. For instance, in Fig. 6, a slight increase of the impedance can be observed in some cases. This is contrary to the main hypothesis that was made in Ref. [27], mostly for simplicity, with a geometrical definition of the impedance variation. A drastic way to show the invalidity of this hypothesis is to consider a reflective BC at the outlet. In practice, experimenters try to achieve an anechoic exit in their aeroacoustic ducts to avoid spurious reflections. However, the anechoicity is never perfect, especially at low frequencies, and reflected waves can parasite the measurements (and a fortiori, any eduction process).

Converged impedances are shown in Fig. 9, for an outlet impedance of $Z_{\text{outlet}} = 3$, which corresponds to a reflection coefficient of 0.5 (proportion of the wave that is reflected back upstream).

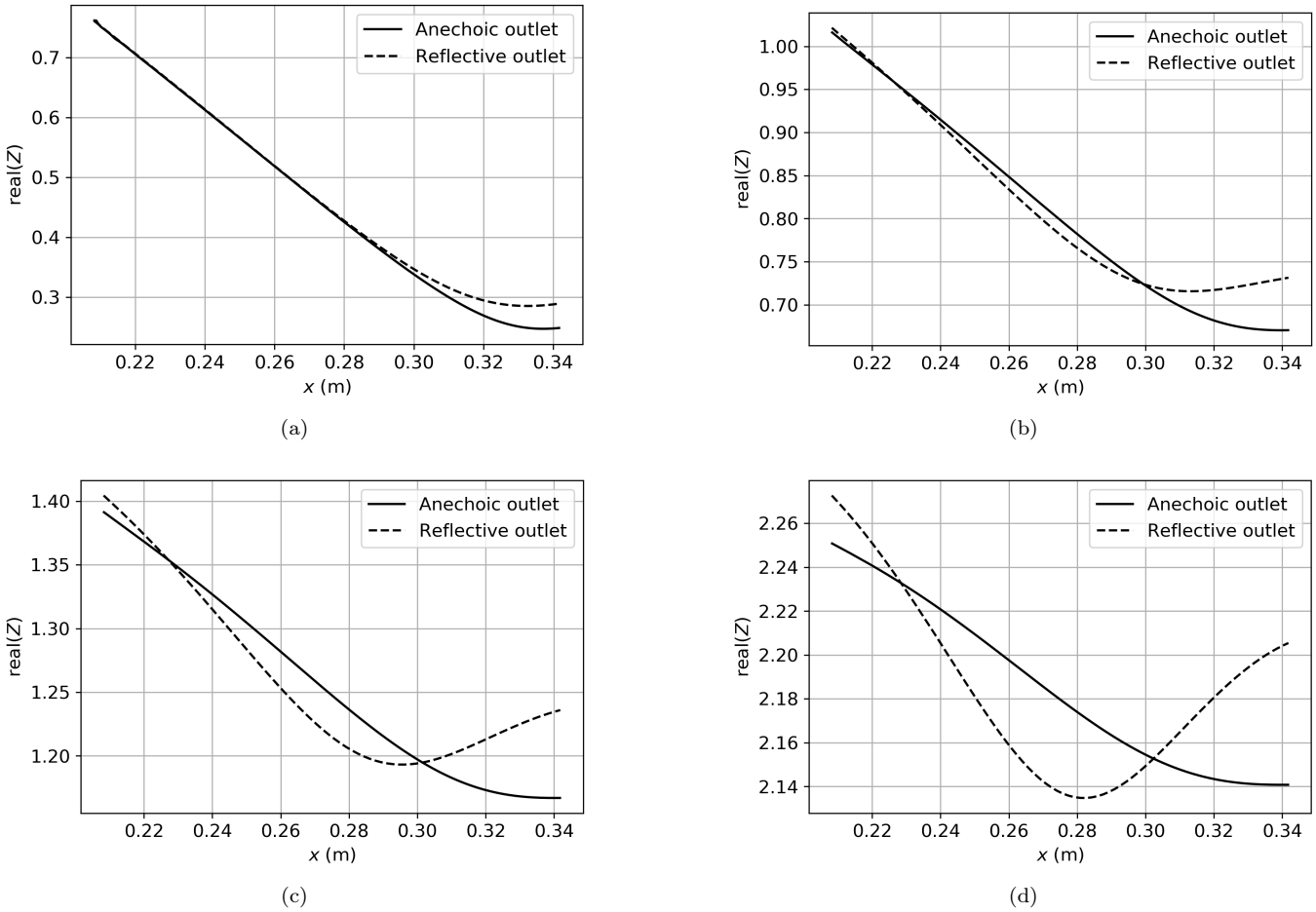

Figure 9: Converged spatially-varying impedances, without flow, in the presence of a reflective outlet BC ($Z_{\text{outlet}} = 3$). The incident wave comes from the left, with incident SPL = 140 dB, $f = 1$ kHz. For all cases, the nonlinear factor is $\alpha_{\text{NL}} = 1.2$. a) $Z_{\text{ref}} = 0.1$; b) $Z_{\text{ref}} = 0.5$; c) $Z_{\text{ref}} = 1$; d) $Z_{\text{ref}} = 2$.

Judging from Fig. 9, the effect of the outlet BC is mostly present for the higher values of liner impedance. The converged fields obtained with both an anechoic and reflective outlets are given in Fig. 10 for $Z_{\text{ref}} = 2$. A secondary peak of normal velocity is evidenced in the reflective case.

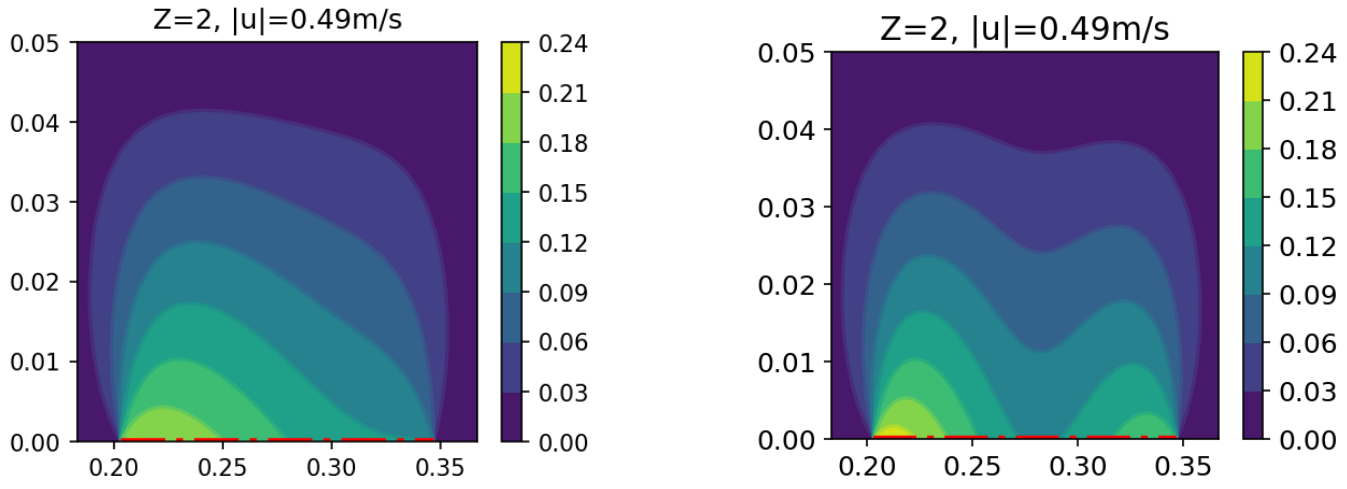

(a) (b)

Figure 10: The $|v|$ field in the $x-y$ plane above a liner with converged spatially-varying impedances, with $Z_{\text{ref}} = 2$. The dashed red line in the 2D plots corresponds to the position of the liner in the duct. No flow is considered. Incident SPL = 140 dB, $f = 1$ kHz, $\alpha_{\text{NL}} = 1.2$. The incident wave is coming from the left (increasing x values). a) Anechoic outlet; b) Reflective outlet.

Since a reflected wave is propagating upstream, it meets the downstream impedance discontinuity and creates another phenomenon of local increase in the nonlinearity. This is coherent, since a higher proportion of the wave reaches the outlet when the liner impedance is high. Indeed, when no flow is considered, such as in the present case, the liner absorbs or reflects the incident wave with an impedance lower than or equal to 1, and is less efficient with higher values of impedance. When a large impedance discontinuity is present (i.e., $Z_{\text{ref}} = 0.1$), a large proportion of the incident wave is reflected at the first impedance discontinuity, back upstream towards the inlet.

It is now clearer why the hypothesis made in Ref. [27] allowed for accurate eduction results: not only was the outlet BC anechoic at the frequencies of interest, but the impedance values were also low, thus limiting the influence of the outlet BC.

4 Experimental validation

The present model is used in an impedance eduction process, taking the same experimental data that were used in Ref [27] (cases 3 and 4). The details of the liner sample and test configurations are succinctly recalled here for completeness, and additional details can be found in Ref [27].

4.1 Liner sample and test configuration

The liner sample was designed within the framework of the International Forum for Aviation Research (IFAR) benchmark challenge #1 [41], and manufactured by an additive process. It has an overall length of 150 mm, and consists in a perforated facesheet of thickness 0.86 mm, backed by a cavity with a core depth of 50.8 mm. The average perforation ratio is 11%, taking into account the partitions, and the perforation diameter is 1.04 mm.

An average Mach number of $M_a = 0.1$ was used in the B2A aeroacoustic bench at ONERA (mass flow rate of 100 g/s at an ambient temperature of $T = 20\,^{\circ}$C and atmospheric pressure conditions), and two experiments were performed. In both cases, a mono-sinus excitation signal was generated at $f = 1528$ Hz, which is close to the resonance frequency of the liner. Two excitation levels are considered for the incident wave, near 140 dB and 147 dB. In the following, these experiments will be coined as "Experiment 1" and "Experiment 2", respectively.

Using the geometrical characteristic of the IFAR sample, one can evaluate numerically the impedance of such a sample, in the absence of a shear grazing flow and in the linear excitation regime. The transfer matrix method is used [42, Chap. 11], and the perforated facesheet is represented by a rigid equivalent fluid [2]. The calculated impedance is given in Fig. 11 as a function of the frequency. A meaningful feature of this liner, in the context of the present study, is that its resistance is very low near the resonance frequency ($\text{re}(Z) \approx 0.04$). Using Guess' [7] and Melling's [6] models, with a perforation rate of 11%, the nonlinear coefficient of Eq. 5 is predicted to be $\alpha_{\text{NL}} \approx 0.2$.

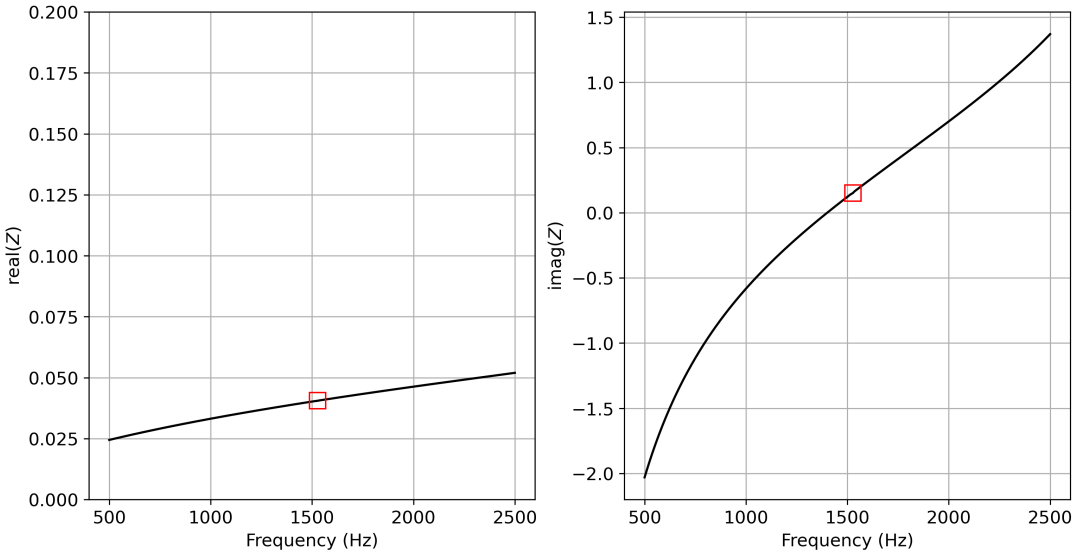

Figure 11: Reference impedance values of the IFAR liner sample as a function of the frequency, evaluated with a rigid equivalent fluid assumption and a transfer matrix method. The red symbols indicate $f = 1528\,\text{Hz}$. $Z_{\text{ref}}\,(f = 1528\,\text{Hz}) \approx 0.04 + 0.21\text{j}$.

4.2 Laser Doppler velocimetry

An LDV equipment is installed in the B2A duct. Using interferometry principles, both the streamwise (x) and vertical (y) total velocity components (u and v, respectively) can be measured. The acoustic part of these signals is extracted from the total velocity measurements, using correlations with the reference loudspeaker signal. The measurement window is located directly above the liner sample, at a distance between 1 mm and 30 mm in the y direction (see Fig. 1). More details on the LDV system and measurements can be found in Refs. [43–45]. Suffices to know that a dense set of points above the liner is used for the measurements of the two components of the acoustic velocity fields, and that these fields are then used as the input data for the eduction process. The experimentally measured source coefficient $|A_s|$ was obtained via a wave sorting procedure using pressure measurements upstream of the lined section. Its value can then be used as a further means to validate the eduction process defined in Sec. 4.3, since the pressure measurements were not used during the eduction. However, the source coefficient phase $\phi\,(A_s)$ is unknown here, as the identified value depends on the location of the inlet in the mesh.

4.3 Eduction strategy

The eduction process is recast as a Bayesian inference problem. The unknown parameters are considered as random variables, and the new quantities of interest are their posterior probability density functions (pdf). These pdf gather the knowledge on parameters, informed by acoustic observations (here, the velocity fields acquired by LDV) and by prior knowledge one might have on the parameters (for example, the passivity condition $\text{re}(Z) > 0$ can be enforced by a Gaussian probability truncated at 0). Details on Bayesian inference can be found in Ref. [46, Chap. 11]. For applications on liner impedance eduction, see e.g Refs. [22, 23]. For completeness, some additional details are given in the following.

4.3.1 Bayesian inference

Using Bayes' theorem, the posterior probability writes

$$\mathcal{P}\,(\boldsymbol{\theta}|\mathcal{D}, I) \propto \mathcal{P}\,(\mathcal{D}, I|\theta)\,\mathcal{P}\,(\theta, I)\,, \tag{6}$$

where $\boldsymbol{\theta} = (\text{re}(Z_{\text{ref}}),\, \text{im}(Z_{\text{ref}}),\, \alpha_{NL},\, |A_s|\,,\, \phi\,(A_s))$ represents the model parameters to identify, $\mathcal{D}$ is the observed data (real and imaginary parts of LDV measurements), and I represents background general information, such as the choice of model (i.e., the LEE for wave propagation here). $\mathcal{P}\,(\boldsymbol{\theta}, I)$ is the prior probability, taken as truncated uniform probabilities to indicate an initial lack of knowledge regarding the parameters to be identified (i.e., blind inference). The *likelihood* $\mathcal{P}\,(\mathcal{D}, I|\boldsymbol{\theta}) = \mathcal{L}\,(\boldsymbol{\theta})$ represents the goodness of fit between the model and the data for a given set of

model parameters, and writes, if the noise is assumed Gaussian,

$$\mathcal{L}(\boldsymbol{\theta}) = \prod_{\substack{g \in [\mathrm{re}(u),\, \mathrm{im}(u),\\ \mathrm{re}(v),\, \mathrm{im}(v)]}} (2\pi\sigma_g)^{-N_g/2}\, e^{-\frac{S_g}{2\sigma_g^2}}, \tag{7}$$

where the g index indicates the observed field. The data noise standard deviation σ_g is assumed constant for all fields ($\sigma_g = \sigma$), and is estimated during the eduction process, along with the parameters in $\boldsymbol{\theta}$. N_g is the number of observed data points for each field. S_g is defined as

$$S_g = \sum_{k=1}^{N_g} |g_k - g_{k,\mathrm{exp}}|^2, \tag{8}$$

where $g_{k,\mathrm{exp}}$ is an experimentally measured field at position k, and g_k is its numerical counterpart, evaluated by the DG solver and including the convergence of the iterative procedure for the evaluation of the spatially-varying impedance (see Sec. 2).

Due to the high numerical cost of performing a Markov Chain Monte Carlo (MCMC) evaluation of the posterior density functions, as was done in Ref. [22], a model reduction was first performed in Ref. [23] based on the snapshot-POD approach [47]. However, in the present case, part of the linear system corresponding to the DG numerical fluxes at the spatially-varying impedance BC needs to be re-created at each iteration required to reach convergence. This precludes the direct use of our previous method. This is all the more prejudicial to the present model, since it requires many evaluations of the direct solver in order to attain convergence, especially when the liner has a low resistance value (this information is *a priori* unknown).

A surrogate model is thus built (see Sec. 4.3.2), with a limited number of evaluations of the likelihood. Then, a MCMC approach based on Refs. [48, 49] (similar to the one we used in Ref. [23]) is used to explore the posterior probability functions of the model parameters.

4.3.2 Surrogate modeling

Bayesian inference requires an expensive exploration of the parameter space, especially in the presence of time-consuming function evaluations or with a high number of parameters. To palliate this problem, a design of experiment (DOE) enrichment strategy is used. The enrichment consists in maximizing an acquisition function, called expected improvement (EI, see Ref. [50]), which yields the next experiment to be added. After each enrichment, a Gaussian process regression model [51] is reconstructed from the enriched DOE. This Gaussian process replaces the expensive evaluation of $\mathcal{L}(\boldsymbol{\theta})$, which includes the iterative process to reach convergence of the spatially-varying impedance (see Sec. 2).

The individual with the best expected improvement is then added to the DOE. Figure 12 illustrates the EI acquisition function to maximize for a parameter x and a function $f(x)$. The probability of improvement is represented by the green area and evaluated from the value of the known minimum of the DOE (dashed red line). The Gaussian process is reconstructed each time a point is added. The enrichment process is repeated until convergence, in an open loop process controlled by the maximum available numerical budget (here, the limit is 1000 calls to Eq. 7). An initial DOE consisting of 200 samples is initialized prior to the enrichment strategy (Latin-hypercube sampling [52]).

4.4 Eduction results

Using the LDV measurements and the eduction strategy of Sec. 4.3, the model parameters of Eq. 5 can be inferred. In addition to the real and imaginary parts of Z_{ref} and of α_{NL}, the source coefficient amplitude $|A_s|$ and phase $\phi(A_s)$ have to be identified as well. The inference is performed in two experiments (Experiment 1 and Experiment 2), that differ only by the acoustic source intensity. These correspond to Cases 3 and 4 in Ref. [27]. The reference case consisting in the constant impedance eduction is also done.

Via the MCMC process, one can evaluate the posterior probability functions (pdf) of all the parameters, as displayed in Fig. 13. These are obtained with the approximate evaluation of the likelihood, using the surrogate model described in Sec. 4.3.2.

The spatially-varying impedances that have been educed (with credibility intervals corresponding to 95% of the variability) are shown in Fig. 14. To obtain converged statistics for the mean and credibility intervals, 200 samples were drawn randomly from the Markov chains, the direct problem described in Sec. 2.2.1 was solved each time, and the impedance was extracted numerically. For these calculations, the surrogate model cannot be used, as it only maps the parameter space onto the likelihood value.

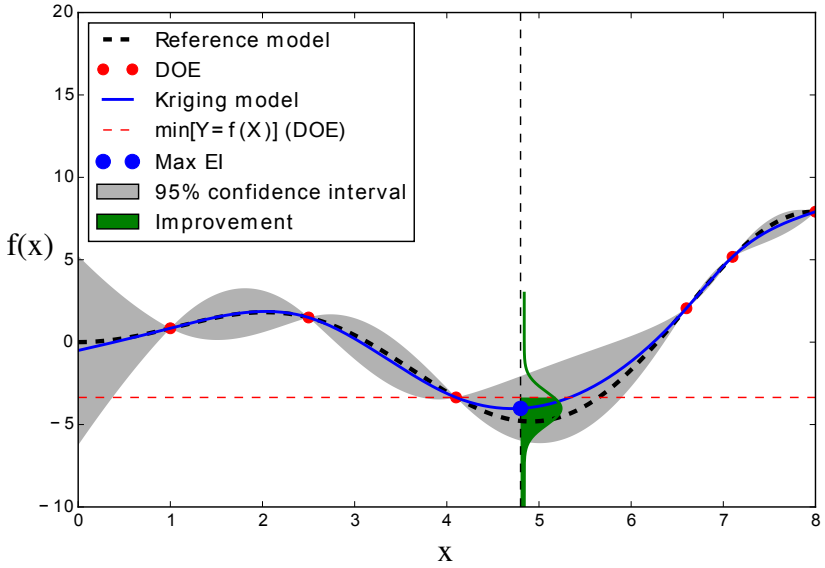

Figure 12: Expected improvement acquisition function.

The constant impedance that was educed is relatively close to the maximum value of the spatially-varying impedance. This suggests, in agreement with the preliminary study in Sec. 3, that the upstream impedance discontinuity is indeed the main parameter in terms of sensitivity to the observed velocity fields. With longer liner samples, the educed constant impedance is expected to be reduced.

A summary of the results is given in Table 1, where the values correspond to the maximum a posteriori estimate (MAP) (i.e., the point of maximum of the left hand side of Eq. 6). The present spatially-varying impedance model is coined "Variable Z", while the reference identification procedure is coined "Constant Z". The cost function is reported to check which model best fits the data, and is simply

$$\text{Cost function} = \sum_{\substack{g \in [\mathrm{re}(u),\, \mathrm{im}(u),\\ \mathrm{re}(v),\, \mathrm{im}(v)]}} S_g, \tag{9}$$

where S_g is defined in Eq. 8 and where lower values correspond to a better fit to the data. There are a some elements

Table 1: Eduction results obtained with LDV measurements. A mono-sinus excitation is used, at $f = 1528\,\mathrm{Hz}$, and a shear grazing flow of average Mach number $M_a = 0.1$ is considered. A wave sorting procedure is used to calculate the true value of the incident wave coefficient $|A_s|$, with 3 microphones placed upstream of the liner. Reference values are obtained using the transfer matrix method, and α_{NL} is obtained with the Guess model [7].

		Experiment 1		Experiment 2	
Model	Reference	Variable Z	Constant Z	Variable Z	Constant Z
Exp. $\lvert A_s\rvert$	–	0.51		1.11	
Cost function	–	0.57	0.95	1.27	3.55
σ	–	0.04	0.05	0.06	0.1
$\mathrm{re}\,(Z_{\mathrm{ref}})$	$4.0 \cdot 10^{-2}$	$3.1 \cdot 10^{-3}$	0.34	$1.1 \cdot 10^{-3}$	$5.2 \cdot 10^{-1}$
$\mathrm{im}\,(Z_{\mathrm{ref}})$	0.15	0.13	0.17	0.03	0.12
α_{NL}	0.2	0.51	–	0.43	–
$\lvert A_s\rvert$	–	0.51	0.52	1.18	1.12
$\phi\,(A_s)$, rad	–	2.02	2.02	1.99	1.82

of interest that can be drawn from Table 1, and that are highlighted next:

- ▷ In both experiments, and with both models, the source amplitude $|A_s|$ has been correctly identified.
- ▷ When a constant impedance is used for the eduction, the educed resistance value is considerably higher than the target reference value. However, for both experiments at different SPLs, the reference resistance $\mathrm{re}\,(Z_{\mathrm{ref}})$ that is identified with the spatially-varying impedance model is similar, and very close to the theoretical value.

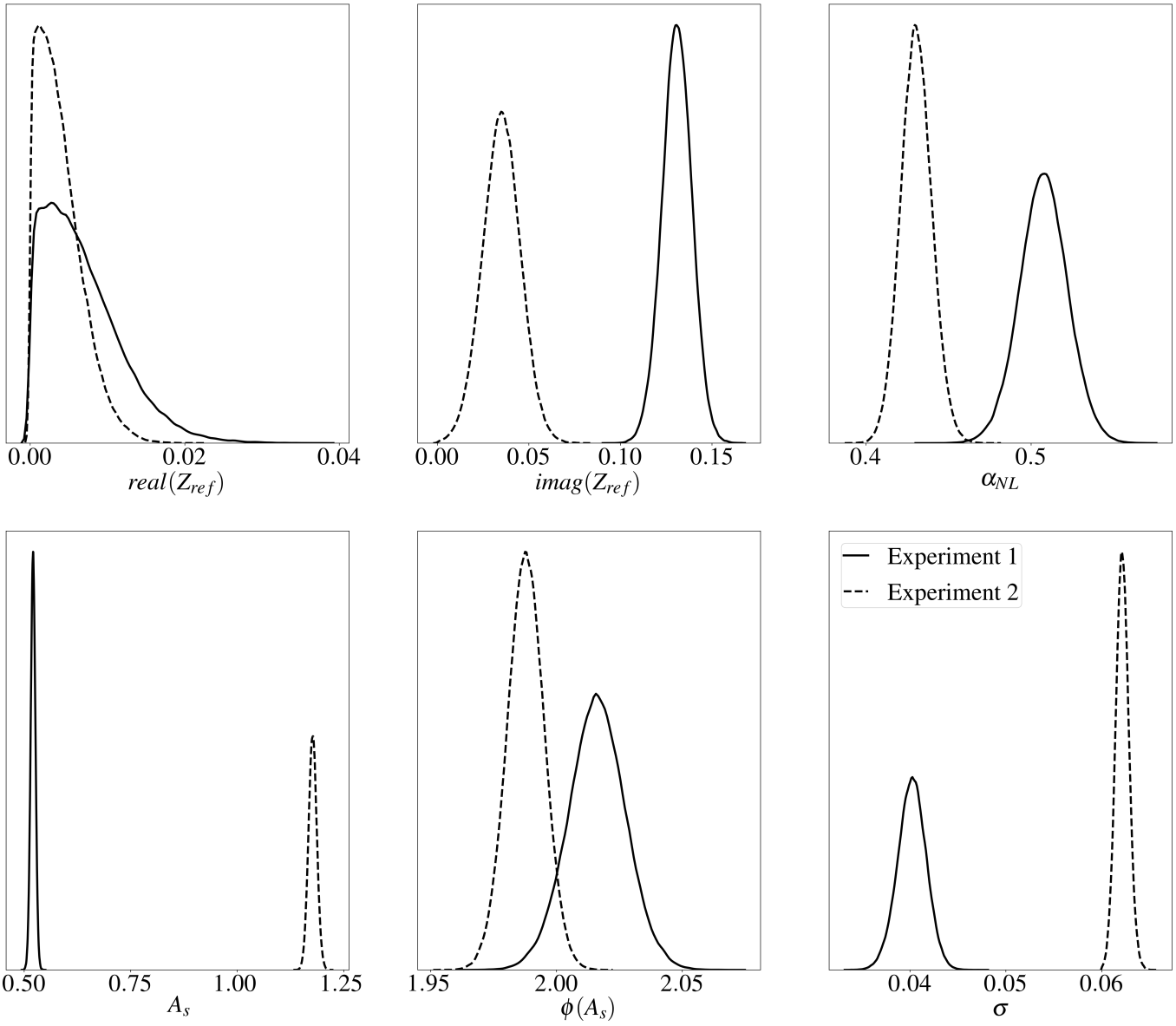

Figure 13: Posterior probability density functions of the educed parameters, in Experiments 1 (140 dB) and 2 (147 dB).

- ▷ The reactance shows coherent values between all identifications (considering that its range of variation is $]-\infty;+\infty[$). A follow-up study could consider a nonlinear variation of the reactance, as a function of $|v_n(x)|$, to perhaps reduce even more the cost function and obtain a nonlinear parameter characterizing the reactance's dependency to the SPL.
- ▷ The nonlinear parameter α_{NL} that was identified with the spatially-varying impedance model is higher ($\times 2-2.5$) than the target reference value. However, the value remains very close from one experiment to another.

This last point could indicate that the nonlinear behavior of the sample differs from that predicted by the Guess and Melling models. The interaction of the shear grazing flow and the SPL nonlinearity could be responsible for an unforeseen increase in the nonlinearity, resulting in a higher educed value of α_{NL}.

A pronounced decrease in the cost function is obtained with the spatially-varying model, even more so in the second experiment where the incident SPL is high. At the expense of one more parameter to identify, the reduction is cost function from the reference constant impedance case is respectively 40% and 64% for Experiments 1 and 2. Note that a higher improvement was indeed expected for experiment 2, where the nonlinear effects are bound to be more marked, due to a higher incident SPL. In Ref. [27], a similar improvement of the cost function was observed on the same data for Experiment 1. However, for Experiment 2, the reduction of cost function was about 83%, compared with the reference case. This superior result is first attributed to a higher number of parameters in the eduction

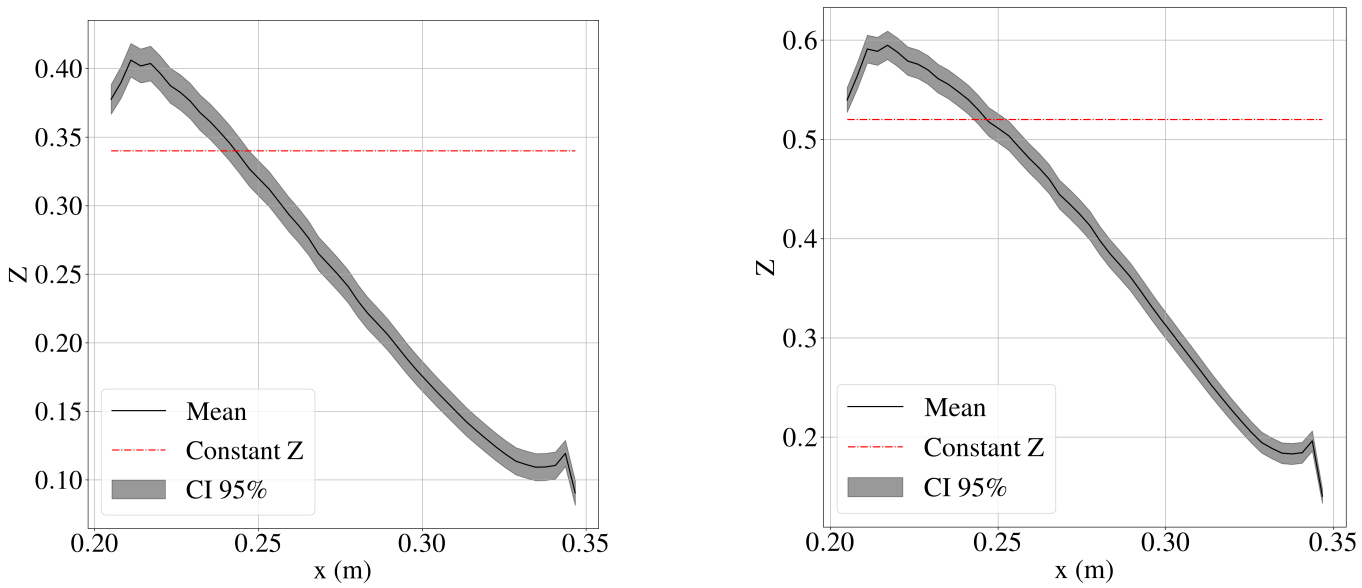

(a) (b)

Figure 14: Educed spatially-varying impedance and 95% confidence intervals. The dashed horizontal line corresponds to the value identified when the impedance is assumed constant spatially. a) Experiment 1; b) Experiment 2.

process of Ref. [27], to define geometrically the spatial variation of the resistance. It is also possible that the model used in the present work (Eq. 5) is not accurate enough to represent all the features of the experimental data.

Comparisons between experimental data and inferred values of the velocity fields are displayed in Figs. 15, 16, at different heights over the liner.

Overall, the goodness of fit is quite marked, indicating that the model is capable of capturing the main features of the experimental data.

4.5 Discussion

The previous experimental investigation showed that it was indeed possible to obtain a better fit to the experimental data with the present iterative model, compared with the constant impedance case, when a high SPL is present. While this is a first element of proof regarding the usability of the present model for impedance eductions, there are still questions that remain unanswered, and that should be tackled in future studies.

Only the case of a mono sinus excitation was used for the eduction process. It is unclear, however, how the model would behave if multiple frequencies were considered, or multiple acoustic modes. While the case has been studied theoretically by Eversman for the direct problem [53], it has not been explored in an impedance eduction context. During such an eduction, it remains to be clarified as to what value of $|v_n(x)|$ should be used.

The proposed model assumes a simple relationship between the nonlinear impedance and the normal velocity field, given in Eq. 5. While this kind of relationship is routinely used for classic acoustic liners with a single degree of freedom, things get more complex when multiple degrees of freedom are considered (i.e., when liners are stacked on one another, in order to extend the frequency range of absorption). In such a case, the first perforated plate, flush with the duct, would not necessarily share the same nonlinear model as the second perforated plate, so Eq. 5 would be missing a term. A solution to this problem would be to use a transfer matrix approach to represent each acoustical unit element, and evaluate the normal velocity at each layer [24].

In this work, LDV measurements were used to perform the eduction process and retrieve the parameters of interest. It seems advantageous to use velocity fields as the input of such a method, especially for the high SPL case where, in particular, the normal velocity fields plays such an important role in the liner's behavior. A challenge to tackle would be that of performing the same study, using only pressure measurements (typically, on the wall opposite the liner, as done in multiple labs already). An advantage of using pressure measurements upstream of the liner (potentially in addition to LDV measurements), would be that the source amplitude and phase could be better characterized with a wave sorting procedure, or included in the eduction process.

The present study highlights a potential reason for variability in eduction results between aeroacoustic benches. When the SPL is high, and if a constant impedance approximation is made, the educed value of the impedance depends

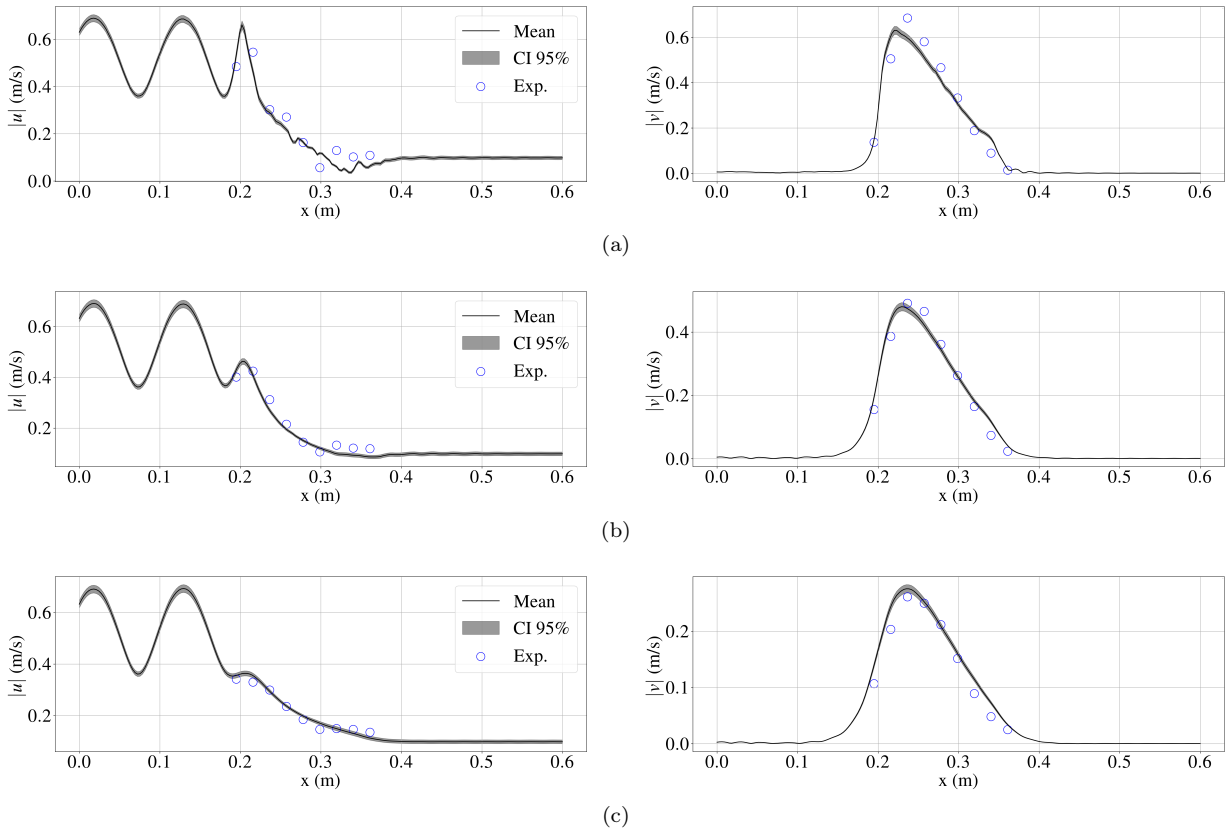

Figure 15: Comparison between experimental and inferred velocity fields in Experiment 1, at different heights y in the B2A. Incident SPL is approximately 140 dB, and the incident wave comes from the left. a) $y = 6$ mm; b) $y = 15.6$ mm; c) $y = 30.4$ mm.

on the length of the liner.

5 Conclusion

This investigation was concerned with the question of how the impedance of an acoustic liner behaves in the presence of a high SPL in aeroacoustic ducts. An iterative model, similar to that of Eversman's [24], was proposed in the harmonic regime to try to account for the space-dependency of the impedance resulting from the nonlinearity. At each iteration, the normal velocity field at the impedance BC was used to update the impedance value, using a generalization of the Melling [6] and Guess [7] models, until a convergence criterion was reached. Different highlights of this model are given below.

- ▷ The impedance discontinuity is a significant driver of the nonlinear response of an acoustic liner at grazing incidence. A pronounced discontinuity tends to locally increase the intensity of the normal acoustic velocity, thus resulting in strong nonlinear effects. For two liner samples having the same nonlinear behavior at normal incidence, a large difference in nonlinear behavior can be observed at grazing incidence if their impedance is different.

- ▷ The convergence of the iteration process is more difficult to reach for low resistivity liners. This is due to a succession of over- and under-predictions of the local normal acoustic velocity at the liner BC, at each iteration.

- ▷ The nonlinear impedance effect is less pronounced in ducts having a lower duct height. This feature is attributed to an averaging of the normal velocity fields, that needs to cancel out at the rigid wall opposite the liner.

- ▷ The direction of the flow relative to the incident wave propagation seems to play a role in the space-dependency of the impedance. When the wave and flow are in the same direction, the average impedance can be higher than when wave and flow are opposite in direction. The exact nature of this deviation remains to be elucidated.

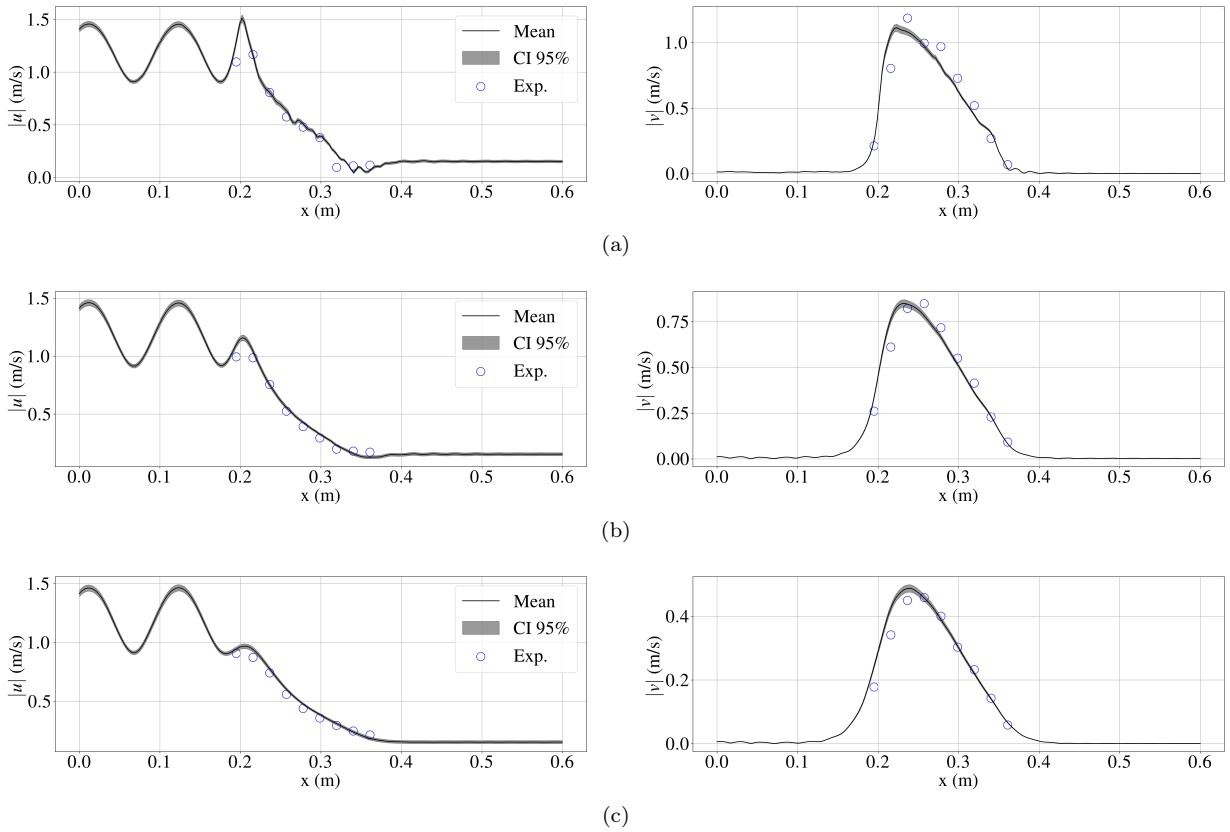

Figure 16: Comparison between experimental and inferred velocity fields in Experiment 2, at different heights y in the B2A. Incident SPL is approximately 147 dB, and the incident wave comes from the left. a) $y = 6$ mm; b) $y = 15.6$ mm; c) $y = 30.4$ mm.

▷ Contrary to our previous assumptions in Ref. [27] or the one in Ref. [28], the spatially-varying impedance field (once converged) is not necessarily a monotonously decreasing function of the space variable. For instance, when the outlet BC is partially reflective, waves propagating back in the upstream direction can "see" the upstream impedance discontinuity and increase the impedance value in the vicinity of the discontinuity.

The iterative model was used in an eduction process based on LDV measurements performed in an aeroacoustic duct near the liner resonance, at a high SPL. Compared with the constant impedance classical model, a reduction in the cost function of up to 64% was observed, indicating an improved goodness of fit to the experimental data. Contrary to previous geometrical assumptions of the impedance field [27, 28], this paper's model only uses known physical relationship linking the particle velocity to the impedance. As a result, the educed parameters are more "intrinsic" to the liner, possibly resulting in a more meaningful information for the liner designer.

The incident SPL is not the only quantity with which one should try to predict the global acoustic response of a liner, at non-normal incidence. Being an integral quantity, the SPL does not see, locally, the normal particle velocity variation at the impedance discontinuities. In addition, one should be careful when designing an experiment and setting an incident SPL value. Locally, the equivalent SPL (based on particle velocity) that is experienced by the liner can be much higher than what the incident SPL would predict, if the liner's resistance is low.

Liner characterizations performed via eductions should now ideally try to decouple the effect of the flow and that of the SPL effects, by identifying model parameters such as a reference impedance and a nonlinear parameter, at different Mach numbers. Up until now, these coupling effects have probably been "hidden" by one or more assumptions, including the one stating that the impedance is a constant function of space.

References

[1] M. Dah-You, Theory and design of microperforated panel sound-absorbing constructions, Sci. Sin. 18 (1) (1975) 55–71. doi:10.1360/ya1975-18-1-55.

[2] N. Atalla, F. Sgard, Modeling of perforated plates and screens using rigid frame porous models, J. Sound Vib. 303 (1-2) (2007) 195–208. doi:10.1016/j.jsv.2007.01.012.

[3] L. Sivian, Acoustic impedance of small orifices, J. Acoust. Soc. Am. 7 (2) (1935) 94–101. doi:10.1121/1.1915795.

[4] R. Bolt, S. Labate, U. Ingård, The acoustic reactance of small circular orifices, J. Acoust. Soc. Am. 21 (2) (1949) 94–97. doi:10.1121/1.1906488.

[5] U. Ingard, H. Ising, Acoustic nonlinearity of an orifice, J. Acoust. Soc. Am. 42 (1) (1967) 6–17. doi:10.1121/1.1910576.

[6] T. H. Melling, The acoustic impendance of perforates at medium and high sound pressure levels, J. Sound Vib. 29 (1) (1973) 1–65. doi:10.1016/S0022-460X(73)80125-7.

[7] A. Guess, Calculation of perforated plate liner parameters from specified acoustic resistance and reactance, J. Sound Vib. 40 (1) (1975) 119–137. doi:10.1016/S0022-460X(75)80234-3.

[8] M. A. Temiz, J. Tournadre, I. L. Arteaga, A. Hirschberg, Non-linear acoustic transfer impedance of micro-perforated plates with circular orifices, J. Sound Vib. 366 (2016) 418–428. doi:10.1016/j.jsv.2015.12.022.

[9] C. K. W. Tam, K. A. Kurbatskii, Microfluid dynamics and acoustics of resonant liners, AIAA journal 38 (8) (2000) 1331–1339. doi:10.2514/2.1132.

[10] C. K. Tam, H. Ju, M. G. Jones, W. R. Watson, T. L. Parrott, A computational and experimental study of slit resonators, J. Sound Vib. 284 (3-5) (2005) 947–984. doi:10.1016/j.jsv.2004.07.013.

[11] J.-M. Roche, L. Leylekian, G. Delattre, F. Vuillot, Aircraft fan noise absorption: Dns of the acoustic dissipation of resonant liners, in: 15th AIAA/CEAS Aeroacoustics Conference (30th AIAA Aeroacoustics Conference), Miami, Florida, USA, 2009, p. 3146. doi:10.2514/6.2009-3146.

[12] J.-M. Roche, F. Vuillot, L. Leylekian, G. Delattre, E. Piot, F. Simon, Numerical and experimental study of resonant liners aeroacoustic absorption under grazing flow, in: 16th AIAA/CEAS Aeroacoustics Conference, Stockholm, Sweden, 2010, p. 3767. doi:10.2514/6.2010-3767.

[13] C. K. Tam, N. N. Pastouchenko, M. G. Jones, W. R. Watson, Experimental validation of numerical simulations for an acoustic liner in grazing flow: self-noise and added drag, J. Sound Vib. 333 (13) (2014) 2831–2854. doi:10.1016/j.jsv.2014.02.019.

[14] Q. Zhang, D. J. Bodony, Numerical investigation of a honeycomb liner grazed by laminar and turbulent boundary layers, J. Fluid Mech. 792 (2016) 936–980. doi:10.1017/jfm.2016.79.

[15] C. Chen, X. Li, F. Q. Hu, Numerical investigation on acoustic energy flux distribution in a lined duct, in: 2018 AIAA/CEAS Aeroacoustics Conference, Atlanta, Georgia, 2018, p. 3778. doi:10.2514/6.2018-3778.

[16] M. G. Jones, W. R. Watson, D. M. Nark, B. M. Howerton, M. C. Brown, A review of acoustic liner experimental characterization at NASA Langley, NASA TP 220583.

[17] A. Tarantola, Inverse problem theory and methods for model parameter estimation, SIAM, 2005. doi:10.1137/1.9780898717921.bm.

[18] M. G. Jones, W. R. Watson, T. L. Parrott, Benchmark data for evaluation of aeroacoustic propagation codes with grazing flow, AIAA paper 2853 (2005) 2005. doi:10.2514/6.2005-2853.

[19] J. Primus, E. Piot, F. Simon, An adjoint-based method for liner impedance eduction: Validation and numerical investigation, J. Sound Vib. 332 (1) (2013) 58–75. doi:10.1016/j.jsv.2012.07.051.

[20] X. Jing, S. Peng, X. Sun, A straightforward method for wall impedance eduction in a flow duct, J. Acoust. Soc. Am. 124 (1) (2008) 227–234. doi:10.1121/1.2932256.

[21] X. Jing, S. Peng, L. Wang, X. Sun, Investigation of straightforward impedance eduction in the presence of shear flow, J. Sound Vib. 335 (2015) 89–104. doi:10.1016/j.jsv.2014.08.031.

[22] Y. Buot de l'Epine, J.-D. Chazot, J.-M. Ville, Acoustical impedance characterization of liners using a bayesian approach, in: Proceedings of Meetings on Acoustics ICA2013, Vol. 19, ASA, Montréal, Canada, 2013, p. 030108. doi:https://doi.org/10.1121/1.4800548.

[23] R. Roncen, F. Méry, E. Piot, F. Simon, Statistical inference method for liner impedance eduction with a shear grazing flow, AIAA Journal (2018) 1–11doi:10.2514/1.J057559.

[24] W. Eversman, Effect of local impedance variation and non-linearity on multiple tone attenuation, Int. J. Aeroacoustics 14 (1-2) (2015) 281–303. doi:10.1260/1475-472X.14.1-2.281.

[25] B. S. Beck, N. H. Schiller, M. G. Jones, Impedance assessment of a dual-resonance acoustic liner, Appl. Acoust. 93 (2015) 15–22. doi:10.1016/j.apacoust.2015.01.011.

[26] R. Billard, G. Gabard, M. Versaevel, G. Tissot, A non-linear impedance model for micro-perforated liners, in: e-Forum Acusticum 2020, 2020.
URL https://hal.inria.fr/hal-03143278/document

[27] V. Lafont, F. Méry, R. Roncen, F. Simon, E. Piot, Liner impedance eduction under shear grazing flow at a high sound pressure level, AIAA Journal 58 (3) (2020) 1107–1117. doi:10.2514/1.J058756.

[28] C. Chen, X. Li, F. Hu, On spatially varying acoustic impedance due to high sound intensity decay in a lined duct, J. Sound Vib. 483 (2020) 115430. doi:10.1016/j.jsv.2020.115430.

[29] C. Geuzaine, J.-F. Remacle, Gmsh: A 3-D finite element mesh generator with built-in pre-and post-processing facilities, Int. J. Num. Meth. Engng 79 (11) (2009) 1309–1331. doi:10.1002/nme.2579.

[30] L. Pascal, E. Piot, G. Casalis, Discontinuous Galerkin method for the computation of acoustic modes in lined flow ducts with rigid splices, J. Sound Vib. 332 (13) (2013) 3270 – 3288. doi:10.1016/j.jsv.2013.01.021.

[31] E. Piot, J. Primus, F. Simon, Liner impedance eduction technique based on velocity fields, in: Proceedings of the 18th AIAA/CEAS Aeroacoustics Conference, AIAA 2012-2198, Colorado Springs, Colorado, USA, 2012. doi:10.2514/6.2012-2198.

[32] J. S. Hesthaven, T. Warburton, Nodal discontinuous Galerkin methods: algorithms, analysis, and applications, Springer Science & Business Media, New York, 2007. doi:10.1007/978-0-387-72067-8.

[33] S. W. Rienstra, D. K. Singh, Nonlinear asymptotic impedance model for a helmholtz resonator of finite depth, AIAA Journal 56 (5) (2018) 1792–1802. doi:10.2514/1.J055882.

[34] S. Rienstra, G. Vilenski, Spatial instability of boundary layer along impedance wall, in: 14th AIAA/CEAS Aeroacoustics Conference (29th AIAA Aeroacoustics Conference), Vancouver, British Columbia, Canada, 2008, p. 2932. doi:10.2514/6.2008-2932.

[35] A. Schulz, C. Weng, F. Bake, L. Enghardt, D. Ronneberger, Modeling of liner impedance with grazing shear flow using a new momentum transfer boundary condition, in: 23rd AIAA/CEAS Aeroacoustics Conference, Denver, Colorado, USA, 2017, p. 3377. doi:10.2514/6.2017-3377.

[36] Y. Aurégan, On the use of a stress–impedance model to describe sound propagation in a lined duct with grazing flow, J. Acoust. Soc. Am. 143 (5) (2018) 2975–2979. doi:10.1121/1.5037585.

[37] Y. Renou, Y. Aurégan, Failure of the Ingard–Myers boundary condition for a lined duct: An experimental investigation, J. Acoust. Soc. Am. 130 (1) (2011) 52–60. doi:10.1121/1.3586789.

[38] R. Kirby, A. Cummings, The impedance of perforated plates subjected to grazing gas flow and backed by porous media, J. Sound Vib. 217 (4) (1998) 619–636. doi:10.1006/jsvi.1998.1811.

[39] Z. Chen, Z. Ji, H. Huang, Acoustic impedance of perforated plates in the presence of fully developed grazing flow, J. Sound Vib. 485 (2020) 115547. doi:10.1016/j.jsv.2020.115547.

[40] A. Goldman, R. L. Panton, Measurement of the acoustic impedance of an orifice under a turbulent boundary layer, J. Acoust. Soc. Am. 60 (6) (1976) 1397–1405. doi:10.1121/1.381233.

[41] M. G. Jones, D. M. Nark, B. M. Howerton, Overview of liner activities in support of the international forum for aviation research, in: 25th AIAA/CEAS Aeroacoustics Conference, Delft, The Netherlands, 2019, p. 2599. doi:10.2514/6.2019-2599.

[42] J. Allard, N. Atalla, Propagation of Sound in Porous Media: Modelling Sound Absorbing Materials 2e, John Wiley & Sons, New York, 2009. doi:10.1002/9780470747339.

[43] M. Lavieille, F. Simon, F. Micheli, Measurement of acoustic quantity fields in duct flow by Laser Doppler Velocimetry., in: Proceedings of the 12th AIAA/CEAS Aeroacoustics Conference, AIAA-2006-2550, Cambridge, Massachusetts, USA, 2006. doi:10.2514/6.2006-2550.

[44] A. Minotti, F. Simon, F. Gantié, Characterization of an acoustic liner by means of Laser Doppler Velocimetry in a subsonic flow, Aerosp. Sci. Technol. 12 (5) (2008) 398–407. doi:10.1016/j.ast.2007.09.007.

[45] O. Léon, E. Piot, D. Sebbane, F. Simon, Measurement of acoustic velocity components in a turbulent flow using LDV and high-repetition-rate PIV, Exp. Fluids 58 (6) (2017) 72. doi:10.1007/s00348-017-2348-4.

[46] R. C. Smith, Uncertainty quantification: theory, implementation, and applications, Vol. 12, Siam, Philadelphia, 2013.

[47] R. Pinnau, Model reduction via Proper Orthogonal Decomposition, in: Model order reduction: theory, research aspects and applications, Vol. 13, Springer, Berlin, Heidelberg, Berlin, Germany, 2008, pp. 95–109. doi:10.1007/978-3-540-78841-6_5.

[48] E. Laloy, J. A. Vrugt, High-dimensional posterior exploration of hydrologic models using multiple-try DREAM(ZS) and high-performance computing, Water Resour. Res. 48 (2012) W01526. doi:10.1029/2011WR010608.

[49] E. M. Shockley, J. A. Vrugt, C. F. Lopez, PyDREAM: high-dimensional parameter inference for biological models in python, Bioinformatics 34 (4) (2017) 695–697. arXiv:https://academic.oup.com/bioinformatics/article-pdf/34/4/695/25117213/btx626.pdf, doi:10.1093/bioinformatics/btx626.
URL https://doi.org/10.1093/bioinformatics/btx626

[50] D. R. Jones, M. Schonlau, W. J. Welch, Efficient global optimization of expensive black-box functions, J. Glob. Optim. 13 (4) (1998) 455–492. doi:10.1023/A:1008306431147.

[51] C. E. Rasmussen, Gaussian Processes in Machine Learning, Springer Berlin Heidelberg, Berlin, Heidelberg, 2004, pp. 63–71. doi:10.1007/978-3-540-28650-9_4.
URL https://doi.org/10.1007/978-3-540-28650-9_4

[52] J.-S. Park, Optimal latin-hypercube designs for computer experiments, J. Statist. Plann. Inference 39 (1) (1994) 95–111. doi:10.1016/0378-3758(94)90115-5.

[53] W. Eversman, Effect of local impedance variation and non-linearity on multiple tone attenuation, in: 16th AIAA/CEAS Aeroacoustics Conference, Stockholm, Sweden, 2010, p. 3825. doi:10.2514/6.2010-3825.